COMPARING AUTUMN PHENOLOGY DERIVED FROM FIELD OBSERVATIONS, SATELLITE DATA, AND CARBON FLUX MEASUREMENTS IN A NORTHERN MIXED FOREST

by

Bailu Zhao

A Thesis Submitted in

Partial Fulfillment of the

Requirements for the Degree of

Master of Science

in Geography

at

The University of Wisconsin-Milwaukee

May 2019

ABSTRACT

COMPARING AUTUMN PHENOLOGY DERIVED FROM FIELD OBSERVATIONS, SATELLITE DATA, AND CARBON FLUX MEASUREMENTS IN A NORTHERN MIXED FOREST

by

Bailu Zhao

The University of Wisconsin-Milwaukee, 2019
Under the Supervision of Professor Mark D. Schwartz

In this project, autumn phenological transition dates and senescence rate (derived from field observation, satellite data and carbon flux measurements) are compared in a northern Wisconsin deciduous forest. Field data cover 2010 and 2012 for the northern site and 2010, 2012 and 2013 for the southern site, with leaf coloration and leaf fall recorded. Satellite indices are EVI and NDVI obtained from the MODIS V006 product via Google Earth Engine platform, covering 2000 to 2017. Carbon flux indices are NEE and GPP covering 1997 to 2017. Field data and normalized satellite data are fitted by a two-section logistic model while carbon data are fitted by a double-logistic model to derive three transition dates and senescence rate parameters. Comparison among these dates and parameters suggests: (a) Generally, the transition dates derived from NDVI is closest to the transitions of leaf coloration and leaf fall; (b) The senescence rate based on NDVI is also closest to the rate of leaf coloration and leaf fall; (c) In year-to-year comparisons, either NEE or GPP can be the least accurate approach in estimating leaf coloration and leaf fall progress; while in long-term comparisons, the accuracy order of EVI, NEE and GPP is variable; and (d) NDVI-based senescence rate is faster, while the senescence rate derived from the other three approaches don’t differ a lot.

Speculations on the reasons for these findings are as follows: (a) canopy senescence is asynchronous, so the timing of first observed leaf coloration from above-canopy and below-canopy can be different; (b) Compared with NDVI, EVI is more sensitive to the subtle canopy change in early autumn and is less affected by soil noise in late autumn, resulting in longer senescence duration; (c) Photosynthesis starts to decrease before visual senescence due to environmental and leaf physiological change, which leads to the bias between field data and carbon data derived transition in early autumn; and (d) The life activities of shrubs and coniferous trees cause carbon exchange to continue changing after deciduous tree senescence terminates.

TABLE OF CONTENTS

LIST OF FIGURES

LIST OF TABLES

1. Introduction

Phenology has various definitions. The basic definition is “the art of observing life cycle phases or activities of plants and animals in their temporal occurrence throughout the year” (Gratani et al., 1986). Furthermore, the US/IBP Phenology Committee defined phenology as “a study of the timing of biological events and their relationship to seasonal climate change” (Gates, 1969), pointing out the connection between phenophase development and environmental conditions. Furthermore, Lieth also treated phenology as an aspect of analysis and management of ecological systems or ecosystems (Lieth, 1974), thus endowing phenology with ecological meaning. Currently, phenological measures “have become prime indicators of documenting altered life cycles due to environmental change in disciplines from biology to climatology, geography, and environmental history” (Demarée & Rutishauser, 2009).

One of the primary goals of studying phenology is to better understand climate change. Climate change has piqued people’s attention for decades. Global temperature has increased by 0.85°C from 1880 to 2012, and the Northern Hemisphere has probably experienced the warmest 30-year period during the last 1400 years (IPCC, 2014). The relationship between phenology and seasonal climate change is one scope of phenological studies (Lieth, 1974). Significant statistical correlations exist among vegetation phenological timing and climate factors, such as surface daily maximum temperature, insolation, and precipitation (Schwartz, 1990; Schwartz & Karl, 1990; Cong et al., 2013; Liu et al., 2016). In mid to high latitude temperature forest regions, temperature and insolation are the prime limiting factors to growth, rather than precipitation(Zhang et al., 2004; Sparks et al., 2006). In South American tropical evergreen forests, radiation could be more important than precipitation (Xiao et al., 2006). Therefore, vegetation phenology in these regions is widely used as an indicator of climate change,

especially climate warming (Schwartz, 1994; Menzel, 2003; Feng & Hu, 2004; Chapman et al., 2005). For example, both satellite data and meteorological models show earlier green-up in the Northern Hemisphere (Myneni et al., 1997; Schwartz, 1998) is associated with an extended growing season length (GSL) in mid-northern latitudes (White et al., 1999), which is evidence of the impacts of global climate change.

A range of methods have been applied to record phenology, such as *in situ* observation (Dahl & Langvall, 2008), satellite data (Reed et al., 1994), carbon flux measurements (Piao et al., 2008), LAI-2000 Plant Canopy Analyzer (Ahl et al., 2006), and PhenoCam network (Richardson et al., 2018). Among these, the first three approaches are popular and discussed in this project. However, each approach has its own properties and more importantly, limitations. In summary, direct field observation describes ground truth most precisely, but the records are spatially and temporally discontinuous, and only focus on individual plants. Conversely, satellite data and carbon flux measurements are temporally continuous and have large spatial coverage, but their resolutions are so coarse that various species and land cover can be included in a single pixel or one carbon tower footprint, resulting in great uncertainties in estimating phenology. Based on these limitations, a comparison among these three approaches is necessary. The questions to answer through these comparisons are:

1. How best to compare satellite data and carbon flux data to *in situ* observation data?
2. How best to evaluate the accuracy of satellite data and carbon flux data in relation to *in situ* observation data?
3. What differences can be found when satellite data and carbon flux data are compared to observation data?

4. What differences can be found when satellite data and carbon flux data are compared to each other?
5. What environmental and physiological factors may explain these differences?

This thesis addresses the above questions in order. The literature review section examines the properties and limitations of *in situ* observation data, satellite data and carbon flux data. The methodology section will focus on question 1 and 2, where data source and data processing procedures will be presented. The results section will answer question 3 and 4, where the accuracy of approaches will be explored. Finally, the discussion section will deal with question 5, where the results will be explained in relation to environmental factors and plant physiological properties.

2. Literature Review

2.1 Studying Climate Change with Phenology throughout the World

Many studies using plant phenology as an indicator of climate change have been conducted in Europe. In Germany, a summary of 50 years of phenological observation data integrated with climate data shows leaf unfolding and flowering stages advanced by 2.5 to 6.7 days per °C in response to warmer springs, while autumn phenology is less influenced by temperature (Menzel, 2003). Similarly, another German study argues that phenophases in Saxony, German would advance by 3 to 27 days on average by 2050, while the trend in autumn is not as obvious as spring and summer (Chmielewski et al., 2005). In Hungary, flowering stage advanced by 3-8 days in response to spring temperature change (Walkovszky, 1998). In Switzerland, long-term observation records have shown obvious earlier spring appearance dates and a relatively weak delay tendency in autumn (Defila & Clot, 2001). An investigation of 943 phenological records in Estonia suggests 5-20 days advance of plant and bird phenophases in spring, which may be a consequence of winter temperatures, radiation change and human impacts (Ahas & Aasa, 2006). Earlier olive flower phenology across Spain is detected via a thermal model (Galan et al., 2005). First flowering dates advanced by 4 days on average per degree in England (Fitter et al., 1995). The earlier beginning of growing season detected by certain species indicate climate change across Ireland (Donnelly et al., 2006). At the continental scale, a study analyzing over 125,000 observation records covering 21 European countries showed 78% of the records reflect earlier leafing, flowering and fruiting stages, which efficiently corresponds with the warming tendency in 19 countries (Menzel et al., 2006). Similarly, an eight-day advance trend of growing season start occurred over the last 30 years across Europe, corresponding to the changes in temperature and circulation (Chmielewski & Rötzer, 2001).

Overall, earlier spring and later autumn were measured in Europe (Menzel & Fabian, 1999). Research based on satellite data also found an 18-day extension of growing season in Eurasia, similarly, because of an earlier spring and later autumn (Zhou et al., 2001).

Similar trends were also shown in North America. Earlier first-bloom tendency occurred in southwestern and central/eastern Wisconsin (Zhao & Schwartz, 2003), and 55 phenophases showed a trend of -0.12 day per year in southern Wisconsin (Bradley et al., 1999). Increasing vegetation cover during the growing season was observed in southeast and upper Midwestern USA (Zhou et al., 2001), together with extended growing seasons due to later autumn in the USA (Dragoni et al., 2011; Dragoni & Rahman, 2012). In Canada, earlier white spruce bud break date was reported (Colombo, 1998); and a long-term regression of phenological observation data indicated an earlier first-flowering trend in Edmonton, Canada, corresponding with El Nino events and ocean temperatures (Beaubien & Freeland, 2000). Generally, the growing season has been extended for 12 days in North America (Zhou et al., 2001) with earlier starts and later ends (Reed, 2006).

In China, among 1263 phenology time series generated by a study, 90.8% showed earlier spring and summer phenology and 69.0% later autumn phenology (Ge et al., 2015). Advanced last spring frost in northeast China and later first autumn frost date in north-central China are reported, consistent with regional temperature records (Schwartz & Chen, 2002). In temperate zones of China, growing season start became 4 days earlier per decade, while growing season end was 2.2 days later per decade (Chen & Xu, 2012).

At the global scale, earlier green-up in the Northern Hemisphere (Myneni et al., 1997; Schwartz et al., 2006) and extended growing season length (GSL) are reported in northern mid-latitudes (White et al., 1999).

All these studies, whether focusing on specific phenophases or the growing season, draw the same conclusion: spring phenophases tend to advance, leading to earlier growing season onset, while autumn phenology shows weaker trends of delay, resulting in later growing season end. These two changes lead to longer growing seasons. This phenomenon is broadly observed across the Northern Hemisphere, which is related to the overall warmer climate during the past few decades.

Table 1. Terms used in following sections

Acronyms	Terms	Category
LP	Landscape Phenology	Large-scale Observation phenology (Liang et al., 2011)
LSP	Land Surface Phenology	Satellite phenology (De Beurs & Henebry, 2004)
NDVI	Normalized Difference Vegetation Index	Vegetation indices (Rouse et al., 1974)
EVI	Enhanced Vegetation Index	Vegetation indices (Huete et al., 2002)
EVI2	Two-band Enhanced Vegetation Index	Vegetation indices (Jiang et al., 2008; Zhang, 2015)
MODIS	Moderate Resolution Imaging Spectroradiometer	Satellite dataset
NEE	Net Ecosystem Exchange	Carbon flux indices
GPP	Gross Primary Production	Carbon flux indices

SOS	Start of season or Start of Spring	Seasonal marker
EOS	End of Season or End of Spring	Seasonal marker

2.2 History of Field observation in Phenological Studies

Visual observation is the conventional approach to studying phenology. One of the earliest phenological records date back to 1180 in China, when Lv Zuqian records the flowering and fruiting date of 24 species in *Gengzi • Xinchou Diary*. The longest phenological record is cherry-tree flowering dates recorded since the 11th century in Japan (Aono & Omoto, 1994; Mikami, 2008). The longest phenological record in Europe, which is also the first systematic UK record, contains plant and bird observation data from 1736 to 1958, covering over two centuries (Margary, 1925; Sparks & Collinson, 2008). Records in Finland can be traced back to 1896 (Linkosalo, 1999).

In 18th century, the first phenological network was established in Sweden, followed by the Swiss network in 1759 (Dahl & Langvall, 2008). During the 19th century, the European network already covered Netherlands, Italy, France, Great Britain, Ireland and Switzerland (Schnelle, 1956). In 1882, German scholar Hoffmann published guidelines for standard observations, facilitating the development of systematic phenological observation networks in Germany and other European countries (Kaspar et al., 2014). In 1957, German phenologist F. Schnelle established the International Phenological Gardens, monitoring plant development in different climate regions (Defila & Clot, 2001).

Currently, phenological observation networks are available in many countries. The earlier mentioned International Phenological Gardens (IPG) now contains 89 gardens in 19 European countries, covering 28 degrees of latitude and 37 degrees of longitude(http://ipg.hu-berlin.de/ipg/faces/index.xhtml). Furthermore, Global Phenological Monitoring (GPM) gardens were set up in 1998, covering countries beyond Europe (Pagenkopf, 2010). In the U.S., the National Phenology Network (USA-NPN) was established in 2007 (USA-NPN National Coordinating Office, 2016), including 908 plant species and around two million plant observation records by 2017 (https://www.usanpn.org/data/dashboard). In China, under the directory of Zhu Kezhen, a Chinese Phenological Observation Network (CPON) was set up in 1963, now covering 30 observation sites and 162 plant species (http://www.cpon.ac.cn/). Othersinclude French Observatory of Seasons (http://www.obs-saisons.fr/), Canada Nature Watch (https://www.naturewatch.ca/plantwatch/map-of-observations/), Nature's Calendar in the U.K. and Ireland (https://naturescalendar.woodlandtrust.org.uk/) and ClimateWatch in Australia (http://www.climatewatch.org.au/).

Numerous phenological studies are based on large-scale long-term observation data from these networks (Beaubien & Johnson, 1994; Linkosalo, 1999; Ahas & Aasa, 2006; Menzel et al., 2006). However, issues related to observation are also discussed. Observation results might be influenced by the observers' backgrounds. Although there are also studies indicating the performance of junior and senior staff in grading plant development are quite similar, botanists do provide a more consistent result compared with non-botanists (Sparks et al., 2006). Moreover, since observational data are limited in coverage, both spatially and in species, and may be temporally discontinuous, it becomes problematic when applying observation data to global studies (Schwartz, 1994).

2.3 Remote Sensing Applications in Phenology Studies

In recent decades, with the advance of remote sensing techniques, satellite images have enabled phenological monitoring to address some of the shortcomings of observation data (Reed et al., 1994), especially monitoring large-scale geographic areas with a high level of accuracy. Together with the development of remote sensing indices and models, it's now one of the most popular approaches in terms of large-scale phenological studies.

A variety of Vegetation Indices (VI) have been developed and used as measures of satellite-derived phenology. The most common VI is the Normalized Difference Vegetation Index (NDVI). Vegetation absorbs most of the energy in the red band while reflecting most of the energy in the near-infrared band. Based on these characteristics, NDVI showing the contrast between red and near-infrared bands was developed as a sensitive indicator of vegetation cover:

NDVI = (NIR-RED)/(NIR+RED)

NDVI corresponds to specific phenophases with models developed to describe such relationships. Current NDVI models include NDVI threshold models, where a threshold of normalized NDVI is used to represent the onset and offset of greenness (0.5 in White 1997, and 0.35 in Krishna & Prasad 2006) or leaf expansion (0.6 to 0.7 in Nagai 2010). NDVI increase models use the intersection of line-smoothed NDVI time series and moving-averaged NDVI time series, together with the curve direction to define the onset and end of greenness (Reed et al., 1994). Minimum NDVI value model uses derivative NDVI time series and define the date when it switches between positive and negative at the beginning and end of the vegetation cycle (Moulin et al., 1997). Finally, maximum curvature models define the points when maximum curvature of smoothed NDVI time series exist to determine onset of vegetation growth, end of growth, onset of senescence, and onset of dormancy (Zhang et al., 2001). Compared to fitted

Fourier series and asymmetric Gaussian function, double logistic fitting, which is built based on the maximum curvature model, has smaller root mean square errors (Beck et al., 2006).

However, there are limitations to NDVI, for example, some factors unrelated to ecosystems may be interpreted as vegetation, such as satellite drift, differences between sensors in different satellites, atmosphere background variations, and cloud contamination may cause bias, whereas temporal resolution may fail to capture detailed monitoring of short-term phenological events (Reed et al., 1994; Zhou et al., 2001). More recently, the enhanced vegetation index (EVI) was developed:

$$EVI = G\frac{\rho_{NIR} - \rho_{red}}{\rho_{NIR} + C_1\rho_{red} - C_2\rho_{blue} + L}$$

where ρ_{NIR}, ρ_{red}, and ρ_{blue} are corrected surface reflectance, L is the canopy background adjustment, C1 and C2 are the aerosol resistance coefficients, and G is a gain factor (Huete et al., 2002). Compared with NDVI, EVI reduces the impact of soil and atmosphere on the vegetation signal while retaining the sensitivity to canopy change. Furthermore, maximal curvature of the logistic-fitted EVI time series model is used to identify seasonal transition points (Zhang et al., 2004) and demonstrates a comparatively high level of accuracy in estimating the timing of full bud burst dates of deciduous forests (Liang et al., 2011; White et al., 2014).

Nevertheless, EVI is designed for sensors with blue bands, while due to data availability, sometimes working with datasets without a blue band is required. Meanwhile, although NDVI requires only red and NIR bands, its reliability is questionable as discussed before. EVI2 has been developed as a substitute to EVI, which can be computed from only red and near infrared bands but performs equally well for phenology compared with EVI (Jiang et al., 2008; Zhang, 2015). The definition of EVI2 is as follows:

$$EVI2 = 2.5\frac{\rho_{NIR} - \rho_{RED}}{\rho_{NIR} + 2.4\rho_{RED} + 1}$$

Despite the constant improvement in VI model accuracy, some limitations persist. Thus, the reliability of remote sensing data have been discussed. To demonstrate the ability of remote sensing phenology to capture *in situ* observations, direct comparisons are often made between them. Nevertheless, the scale differences between the data derived from remote sensing pixels and field observations inhibits those comparisons. In addressing this problem, gap-filling approaches are necessary. For example, White et al. compared Landsat TM images to extensive field observations (White et al., 2014), and Liang and Schwartz (2009) used land surface phenology (LSP) to hierarchically upscale the field individual-level observation data to community-scale phenological records. Using these techniques and applying these methods can indicate the accuracy of remote sensing data capturing *in situ* vegetation phenology.

2.4 Applying Carbon Flux Measurements to Phenology

Carbon flux is the transfer of carbon from one carbon pool to another (Karsenty et al., 2003). Vegetation plays an important role in the carbon exchange between the biosphere and atmosphere, mainly through photosynthesis (as carbon up-take activity) and respiration (as carbon emission activity). Light plays an important role in photosynthesis and it is also the physical foundation of satellite imagery. Consequently, light transmission processes link satellite data, carbon flux and plant physiology together. Specifically, solar radiation reaches canopies, with part of the spectrum absorbed or transmitted and another part reflected back. The reflected radiation is then detected by satellite sensors to produce satellite images. On the other hand, for the radiation absorbed, part is functional for photosynthesis, which is called absorbed photosynthetically active radiation (APAR, Goetz et al. 2000). APAR provides source energy for

primary production, with the carbon assimilation amount per unit APAR varying among species, plant morphological features, phenology and environment (Tucker & Sellers, 1986; Hunt & Running, 1992; Goetz & Prince, 1996; Cramer et al., 1999; Wehr et al., 2016).

To monitor carbon flux, energy flux and water flux as well as improve the accuracy of satellite-estimated flux indices, an international network called FLUXNET (covering 526 sites on five continents) was established (Baldocchi et al. 2001, Figure 1). Eddy covariance is the most popular carbon flux measurements method in the FLUXNET system. It's suitable for steady and open landforms with relatively uniform vegetation. The above-canopy sensor detects net matter exchange between vegetation and the lower atmosphere. Errors arise from atmosphere, surface and systematic or random instrumental effects (Goulden et al., 1996; Running et al., 1999). Since the eddy covariance method is designed to measure NEE, which is also determined by autotrophic respiration and heterotrophic respiration apart from gross production (Goetz & Prince, 1999), additional environmental measurements and models are required to estimate GPP (Lasslop et al., 2010).

Since both carbon flux measurements and satellite data are open-accessed, globally covered datasets, and are fundamentally related by light transmission, estimating carbon flux by satellite data across various scales are possible. For example, net primary production can be estimated by Advanced Very High Resolution Radiometer (AVHRR) data and a semi-mechanistic GLO-PEM model (Goetz et al., 2000; Cao et al., 2004); Cramer et al. compared 17 biochemical models and satellite-based models in estimating net primary production , finding net primary production pattern and net primary production-climate relationship are consistent globally (Cramer et al., 1999); Running et al. discuss the potential of Earth Observing System (EOS), of which the primary data source is MODIS images, to be integrated with flux

measurements (Running et al., 1999); similarly, Moran et al. discuss the potential of applying satellite data and ground measurements to estimate biomass production (Moran et al., 1995). On the other hand, comparison between these two measurements in phenology studies is also popular. Myneni used NDVI as the indicator of growing season and suggests there are significant statistical correlations among NDVI variation, biomass and carbon dioxide variation (Myneni et al., 1997; Myneni et al., 2001). The Northern Hemisphere growing season estimated from net primary production, NDVI and carbon uptake is generally consistent, suggesting stronger photosynthesis activity (Angert et al., 2005). A phenology index derived from NDVI and NDII (normalized difference infrared index) shows agreement with carbon flux measurements in terms of SOS and EOS (Gonsamo et al., 2012).

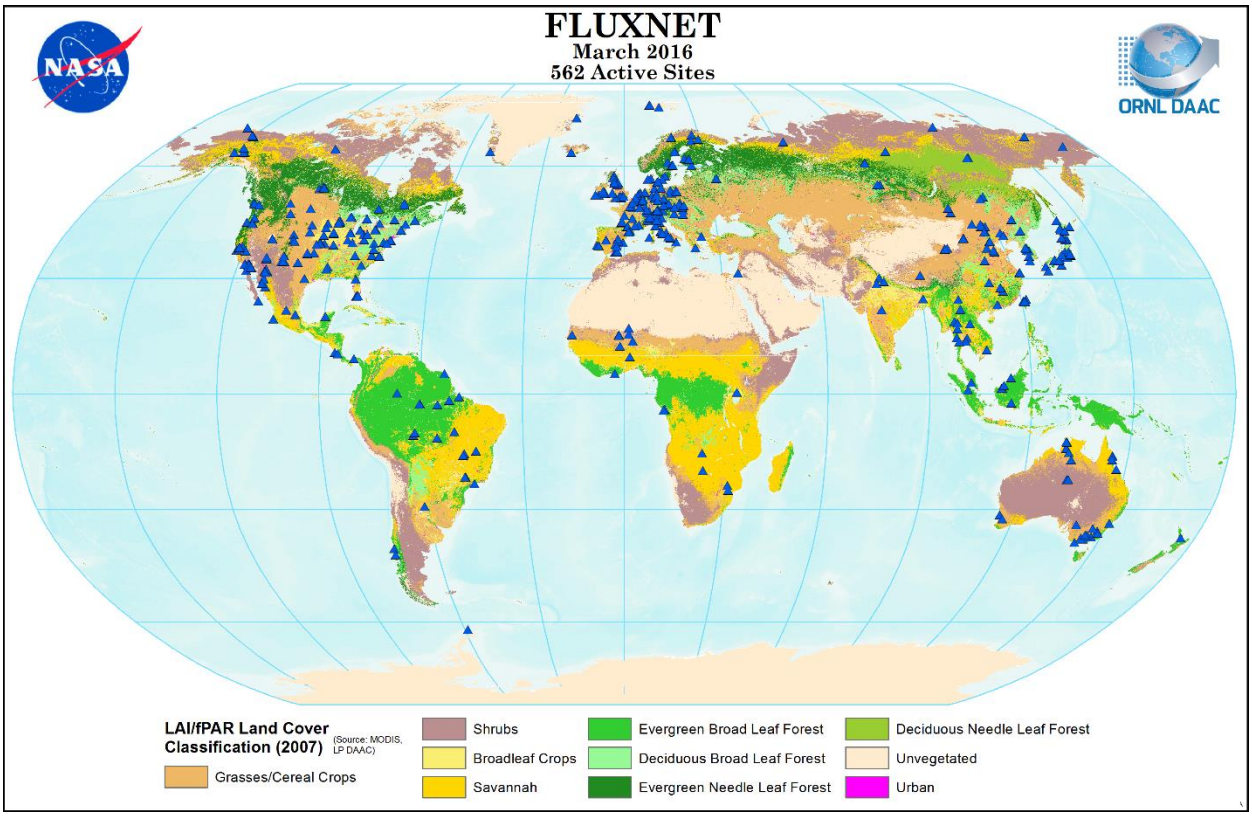

Figure 1. 562 active FLUXNET sites in 2016.

Data source: Falge, E., M. Aubinet, P.S. Bakwin, D. Baldocchi, P. Berbigier, C. Bernhofer, T.A. Black, R. Ceulemans, K.J. Davis, A.J. Dolman, A. Goldstein, M.L. Goulden, A. Granier, D.Y. Hollinger, P.G. Jarvis, N. Jensen, K. Pilegaard, G. Katul, P. Kyaw Tha Paw, B.E. Law, A. Lindroth, D. Loustau, Y. Mahli, R. Monson, P. Moncrieff, E. Moors, J.W. Munger, T. Meyers, W. Oechel, E.-D. Schulze, H. Thorgeirsson, J. Tenhunen, R. Valentini, S.B. Verma, T. Vesala, and S.C. Wofsy. 2017. FLUXNET Research Network Site Characteristics, Investigators, and Bibliography, 2016. ORNL DAAC, Oak Ridge, Tennessee, USA. https://doi.org/10.3334/ORNLDAAC/1530

As for the connection between carbon flux and forests, multiple studies suggest temperate forests work as a major carbon sink (Goulden et al., 1996; Schimel et al., 2015), while the capability of carbon storage varies with stand age, successional diversity, stem radius, and height (Gower et al., 1996; Baldocchi et al., 2001; Caspersen & Pacala, 2001; Desai et al., 2005). Since both vital paths of carbon flux (photosynthesis and respiration), are physiologically related to the stage of leaf growth and senescence in terms of chlorophyll content and carbon assimilation capability, annual carbon flux variation is then linked with plant phenology (Goulden et al., 1996; Falge et al., 2002; Wehr et al., 2016). Importantly, advanced spring vegetation activity caused by warmer springs will lead to increased spring carbon uptake, which is offset by less summer uptake due to hot and dry conditions (Angert et al., 2005; Wolf et al., 2016). Richardson et al. found that prolonged duration of the start and end of season results in a simultaneous increase in gross ecosystem production and evaporation rate, further leading to a slower increase in net ecosystem production (NEP) (Richardson et al., 2010). Autumn phenology also plays a role in carbon flux, as the quantitative relationship between photosynthesis and respiration in autumn will influence annual carbon accumulation. For instance, Dragoni et al. reported an extended autumn and extended growing season, then suggesting this change in phenology explains 50% of the annual carbon flux variation (Dragoni et al., 2011). Piao et al. reports

increasing photosynthesis and respiration due to warmer autumns, with respiration overriding photosynthesis and offsetting 90% of increased spring carbon uptake (Piao et al., 2008).

This consistency between phenology and carbon flux makes estimating phenology transition dates from carbon flux indices possible (Cleland et al., 2007). Models designed for this target can be roughly divided into two types: threshold models and fitting models. Threshold models define phenological transition dates as the intersection of carbon flux indices curves and a pre-defined threshold. For example, transition points between positive and negative NEE values can be treated as the dates of SOS and EOS (Richardson et al., 2010; Garrity et al., 2011; Wu, Chen, et al., 2013; Wu et al., 2017). Threshold models defining the Spring green-up derived from a GPP threshold method shows good agreement with MODIS EVI data (Peng et al., 2017). As to GPP, multiple methods are available to define the transition line of the growing season, for example, a constant threshold of 1 g C m^{-2} day^{-1}, a threshold of 10% of maximum annual GPP value, or degree-day indicator and cumulative temperature sum (Wu, Gough, et al., 2013) .

Like satellite data, two-section logistic fitting models can also be applied to carbon flux data (Liu et al., 2017), and the points with swift transitions are taken as seasonal markers. In addition, double-logistic models developed from two-section logistic models are also applicable. A description of double logistic model is given in Fisher et al. (2006), where a two-section logistic model is simplified into a single curve composed of two logistic components, with one minus and the other one positive. However, this model is still applied to VI indices. Later, Soudani et al. (2008) rewrote this double-logistic function into an asymmetric double-sigmoid function, with a hyperbolic tangent subfunction. The rewritten function enables researchers to derive two inflection points when NDVI is in the middle of its amplitude directly from fitting parameters. Then Garrity et al. (2011) applied this function to carbon flux measurements, and

further derived six inflection points from it. However, different from Zhang et al. (2003), the inflection points in this case are defined by the minimum and maximum of the second derivative, not the change of curvature.

Annual carbon flux variation has biases when estimating phenophases for three reasons. First, as discussed earlier, eddy covariance measurements will inevitably include environmental or instrumental error. Moreover, eddy-covariance measurement has strict requirements for the terrain and vegetation type, which are unlikely to be obtained in the real world. Under less than ideal conditions, large errors may occur (Baldocchi, 2003). Second, eddy-covariance measured NEE values are also influenced by other factors such as soil microbial respiration (Shi & Marschner, 2017) and human activity (Solaymani, 2017). Even for an ecosystem in which the functional vegetation cover is identified as deciduous forest, other ecosystem components will certainly influence the carbon budget. Third, the footprint of eddy covariance towers usually varies between 1.1 and 5 km^2 around the tower (Chen et al., 2011). As a result, this measurement tends to reveal a large-scale, regional average of all ecosystem activities, encompassing many species differences and spatial distribution patterns.

2.5 Crucial Seasonal Markers Showing Phenological Stages

In terms of phenology, spring and autumn phenophases are key parameters because they indicate the start and end of the growing season respectively and impacts of climate change on vegetation can be detected through recording variations in the timing of spring and autumn phenological events. Spring phenological processes include bud, shoot, stem, leaf and flower development (Group, 2001; Yu et al., 2016), while autumn phenology includes both fruiting and leaf senescence stages (Liu et al., 2015). Start of season (SOS) in spring and end of season (EOS) in autumn are used as two markers of growing season duration derived from VIs. Based on the

models applied, SOS and EOS correspond with certain ground-based phenophases. For example, spring indices (SI) models estimated SOS corresponding with first-leaf date or first-bloom date (Zhao & Schwartz, 2003), EVI-based SOS (computed with a logistic function) corresponded with deciduous full bud burst dates (Liang et al., 2011; White et al., 2014), and a spring NDVI threshold of 0.5 matched leaf emergence dates (White et al., 1997).

Seasonal markers are not limited to SOS and EOS. Reed also defined time of maximum NDVI as a marker (Reed et al., 1994). Later, with the earlier mentioned algorithm detecting the day-of-the-year dates of maximal curvature, seasonal markers are further broadened into eight transition points: green-up onset, green-up stability, maturity onset, maturity stability, senescence onset, senescence stability, dormancy onset, and dormancy stability--providing a more comprehensive overview of annual phenology variation (Zhang et al., 2001). Depending on the study goals, these eight seasonal markers can be simplified into four: green-up onset, maturity onset, senescence onset and dormancy onset (Zhang et al., 2004).

2.6 Significance of Autumn Phenology

Compared with spring phenology, autumn phenology has been less studied. In the purview of climate change, the number of studies on how climate factors impact spring phenology exceeds the number of such studies on autumn phenology (Richardson et al., 2006; Donnelly et al., 2017). Nevertheless, autumn phenology is complicated, and the discoveries of spring phenological research can’t be simply applied to autumn. For example, a NDVI threshold of 0.6-0.7 may correspond with the spring leaf expansion stage, while no suitable NDVI threshold in autumn could be defined for a certain phenophase (Nagai et al., 2010). Remote sensing and PhenoCam are more consistent in spring than in autumn (Zhang et al., 2018). Similarly, satellite-derived mid-senescence has little overlap with observed leaf coloration

(Donnelly et al., 2018). Although spring phenological advance is broadly observed, the autumn delay trend is always weaker (Defila & Clot, 2001; Chmielewski et al., 2005; Menzel et al., 2006). Furthermore, lack of understanding about autumn senescence mechanisms (White et al., 2002) inhibits the development of reliable models. Temperature plays an important role in spring phenology (Caffarra & Donnelly, 2011; Caffarra et al., 2011), while not as clear an effect in autumn (Schaber & Badeck, 2003). Nevertheless, some studies argue temperature increases may delay autumn phenology (Menzel et al., 2003). As to precipitation, there is a study suggesting no clear relationship exists between EOS and precipitation (Dragoni & Rahman, 2012), as well as a study asserting that drought in summer and autumn may lead to earlier leaf coloring and leaf fall (Chmielewski et al., 2005). Some scholars indicate chilling time and photoperiod might control leaf senescence, though models introducing chilling time as a variable are less accurate in predicting autumn phenophases than those using temperature to predict spring phenophases (Richardson et al., 2006; Yu et al., 2016).

Although studies of autumn phenology are restricted by the accessibility of previous work and the complexity of physical mechanisms, autumn phenology still plays an important role in the carbon budget between atmosphere and biosphere, as discussed in the carbon flux section. However, what one can conclude for now is the clear need for further research on autumn phenology.

3. Study Area

The study site is in the Park Falls Range District of the Chequamegon National Forest of northern Wisconsin, where the vegetation type is characterized as a mixed temperate/boreal forest with both deciduous (70%) and coniferous (30%) species (Haugen et al., 1998). The land cover type within the footprint of this tower is identified as mixed forest while the net primary production land cover type and land function type are classified as deciduous broadleaf forest. Annual daily average temperatures range from -18°C to 25°C, with annual precipitation lowest in February (21mm) and highest in August (114mm) (http://www.intellicast.com/Local/History.aspx?location=USWI0531). There were two study plots with slightly different vegetation composition. The north study area is an upland forest dominated by sugar maple (*Acer saccharum*), red maple (*Acer rubrum*), basswood (*Tilia americana*), balsam fir (*A. balsamea*) and white cedar (*Thuja occidentalis*). The south study area is a lowland forest dominated by quaking aspen (*Populus tremuloides*), speckled alder (*Alnus rugosa*), red maple, white birch (*Betula papyrifera*), balsam fir (*A. balsamea*), white cedar (*Thuja occidentalis*) and red pine (*Pinus resinosa*, Hanes 2011).

These study sites are mainly composed of 80-year-old mature hardwood forest which is representative of a significant northern temperate carbon sink and are within the footprint of a 447-m WLEF AmeriFlux tower (45.94°N, 90.27°W, 473m in elevation), which has been operated by the Chequamegon Ecosystem Atmosphere Study group (ChEAS) to record carbon flux data since 1995 (Desai 2005). The WLEF tower is included in NASA's Earth Observation System (EOS) and NOAA's Climate Monitoring and Diagnostics Laboratory (CMDL) network, thus, enough related research and source data relating to this region are available (Liang 2009, https://ameriflux.lbl.gov/).

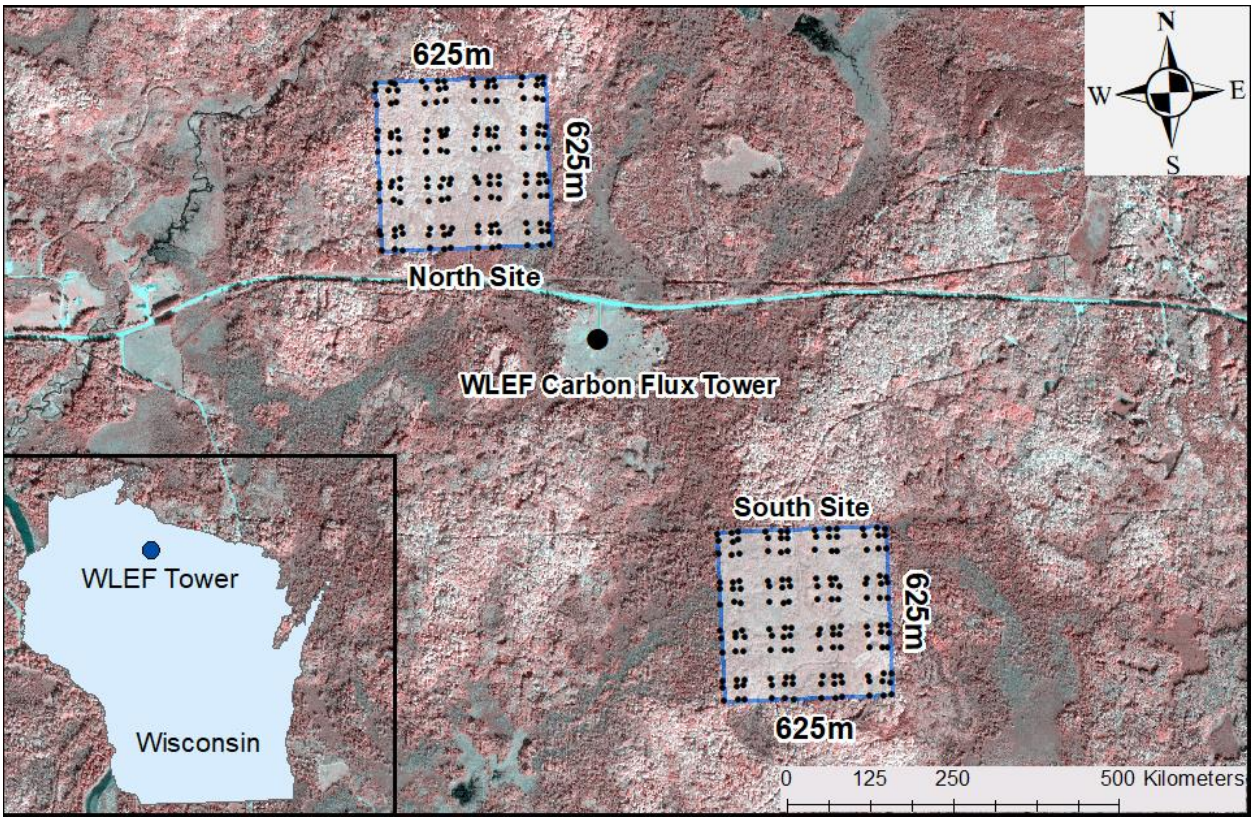

Figure 2. Study Site.

This map was generated by QuickBird (2.4m) false color composite (September 27th, 2012). The black lines are the boundaries of the northern and southern study sites, with the WLEF Flux Tower in the middle of the

4. Data Source and Methodologies

4.1 Data collection

4.1.1 Field data

Field data were collected during 2010-2013, which will be used to evaluate the accuracy of the RS and carbon flux approaches in estimating autumn phenology. Specifically, for the northern sites, autumn phenological data were available for 2010 and 2012; and for the southern sites, data were available for 2010, 2012 and 2013. Field data collection was conducted in two 625m*625m areas, using a two-dimensional cyclic sampling scheme (Burrows et al., 2002). A 3/7 cyclic scheme was applied for longitudinal and latitudinal dimensions to the whole 600m*600m area, with 25m as the unit of sampling space. Within each sampling plot, the three largest trees of the dominant species within a 10-meter radius were selected (each yellow point in Figure 1 represents for a 10-meter radius circle) and monitored regularly. The information on field data collection is available on Table 2.

Table 2. Field data collection information

Site	Year	Number of trees used	Collection period (DOY)	average collection frequency (days)	Collection frequency range (days)	Phenophases recorded
North	2010	336	263-291	3.5	1~4	Leaf coloration and leaf fall
North	2012	335	260-294	4.25	4~5	
South	2010	274	265-293	4	4	
South	2012	270	262-292	4.29	4~5	
South	2013	264	256-291	2	2~3	

The phenophases are recorded using a quantity protocol drawing from the German Biologische Bundesanstalt, Bundessortenamt, and Chemical Industry scheme (BBCH), but adapted to fit the phenology merits of native species (Liang et al., 2011). The scheme is described as follows:

Autumn scheme (Schwartz, 2003; Yu et al., 2016):

800 =Leaf coloration <10%

810 =Leaf coloration 10~50%

850 =Leaf coloration 50~90%

890 =Leaf coloration >90%

900 =Leaf fall <10%

910 =Leaf fall 10~50%

950 =Leaf fall 50~90%

990 =Leaf fall >90%

4.1.2 Satellite data

To derive phenology from satellite data, several criterions should be met. First, enough radiometric resolution is available to produce the vegetation indices. Second, sufficient temporal resolution exists to mitigate cloud cover interference. Among all the available sensors, only SPOT (Vegetation sensor), NOAA, and MODIS meet these requirements, with MODIS having superior spatial and radiometric resolution compared to the other two. The MOD13Q1 006 NDVI and EVI products, with 250m 16-day resolution, are broadly applied to acquire phenology data (https://lpdaac.usgs.gov/dataset_discovery/modis/modis_products_table/mod13q1_v006). In this project, the MOD13Q1 006 dataset was selected for processing satellite-based phenology.

4.1.3 Carbon flux data

Carbon flux data are available on the AmeriFlux website (http://ameriflux.lbl.gov/). The tower provides one-hour interval carbon flux measurements including original (deficient) NEE, GPP records and gap-filled NEE, GPP records, with the gap-filled record dating back to 1996. No data is available for autumn 2005, so this year is not included in the analyses. In addition, the carbon tower didn't operate in the latter half of 2010, and the gap-filled data is problematic with an apparent abnormal decrease, so autumn 2010 carbon data are also omitted.

Table 3. Data summary

Data type	Category	Indices/phenophases	Time period	Footprint
Field data	Direct	Leaf coloration Leaf fall	North: 2010, 2012 South: 2010, 2012, 2013	Point data
Satellite data	Indirect	NDVI, EVI	2000-2017	250m*250m
Carbon flux	Indirect	NEE, GPP	1997-2017 (no 2005, 2010)	5km radius

4.2 Methodologies

4.2.1 Deriving landscape phenology

Landscape phenology (LP) is derived from leaf coloration and leaf fall time series to represent field observation-based phenology. The methodology is described in Liang and Schwartz (2009). Basically, the procedure can be divided into two parts: a) determination if spatial autocorrelation exists, and b) hierarchically upscaling of field phenology data if no spatial autocorrelation is found.

The examination of spatial autocorrelation aims to reveal if vegetation phenology follows Tobler's First Law of Geography: Everything is related to everything else, but near things are more related than distant things. Spatial autocorrelation in phenology would indicate that the

environmental factors in this study area have a significant impact on plant phenology, which overrides the between and within species differences determined by genes. If not, then the opposite conclusion will hold. In previous studies, spatial autocorrelation was not found (at the 25m scale of these data) in either spring or autumn phenology (Liang et al., 2011; Liu et al., 2015). Therefore, it is reasonable to assume that between and within species genetic difference play a more important role than environmental factors in phenology development at this scale.

Based on this result upscaling can be performed as follows:

First, derive population phenology, which is simply calculating the arithmetic average of individuals of each species since no spatial autocorrelation adjustment is needed.

Second, derive community phenology. Considering the various species and environmental components in different communities, the phenology in each community is calculated separately. The manipulation can be divided into two steps: delineating the boundaries of communities and getting the proportion of each component within each community; and applying a weighted average algorithm for each community. For the first step, community boundary information was obtained from previous work by Liang (2009), where a 1m resolution merged IKONOS image was applied to generate a highly-supervised community classification output. The components in the study areas are categorized into deciduous, coniferous and bare land. Then two QuickBird images were used to conduct a subpixel classification, with multitemporal linear spectral unmixing models adopted. The community boundary file and subpixel classification file are overlaid to get the proportion of deciduous, coniferous and bare land in each community. For the second step, the dominant deciduous species phenology in each community are averaged, then multiplied by the deciduous proportion obtained in the first step to get the community phenology. For communities with relatively large proportion of shrubs, grass

and open canopies, speckled alder is included as a substitute. Evergreen coniferous species are not included in the calculation since they don't show observable phenology in autumn.

Finally, landscape phenology is derived in two steps. First, calculate the average community phenology weighted by community areas. Second, divide the average by deciduous proportion in the entire study area to eliminate unit issues.

Raw landscape phenology time series are be kept since it is the most precise description of what is happening on the ground. However, each time series, representing leaf coloration or leaf fall, is fitted to a logistic model. This is based on the following considerations:

First, when fitting landscape phenology with logistic model, the goodness of fit is high, the time series, indicating fitting model will influence the precision of raw data in an acceptable degree.

Second, the parameters derived from the fitted model provide information on the senescence rate and peak time which raw data series omit. These parameters can be used to compare with the other two approaches.

Third, the model fitting equation can be used to estimate the phenology stage at any given DOY. Different from satellite data and carbon flux measurement, the estimation results provide information with specific phenology significance, which is the percentage of leaves reaching coloration or fall stage. With this information, real-time ground-based data correspondence with satellite or carbon flux derived start of autumn (SOA), middle of autumn (MOA) or end of autumn (EOA) becomes possible.

Finally, for satellite and carbon flux measurements, the model derived transition dates correspond to dates when the rate of senescence accelerates or slows down, rather than the dates when senescence first occurs or stops. Therefore, applying fitting model to field data also returns

dates when the rate of leaf coloration or leaf fall suddenly accelerates or slows down. By doing so, comparing transition dates among different datasets with fixed physical and mathematical meaning are possible, and retains consistency among the approaches. Meanwhile, the DOY when start or end of leaf coloration or leaf fall are first observed can still be determined from raw field data.

4.2.2 Deriving satellite phenology

a. Acquiring and pre-processing satellite data based on the Google Earth Engine platform

In this project, MODIS006 vegetation index (VI) data were selected for deriving satellite phenology. In contrast to conventional data processing procedures, the Google Earth Engine (GEE) was used for easier data access and processing. GEE is a cloud-based platform which enables users to process large datasets with a limited number of lines of codes (Gorelick 2017). An online Integrated Development Environment (IDE) based on JavaScript API is available, and the provided python API makes it possible to code offline in a python environment (https://developers.google.com/earth-engine/). In this project, coding was based on online IDE. The GEE platform proved beneficial to this project for following reasons:

1. The data covers a relatively long duration (1997 to 2017) and since the temporal resolution of the MODIS data is 16-days, roughly 24 images will be needed each year. As a result, conventional downloading will require up to 100GB of storage, and manipulating nearly 500 layers would be labor intensive. However, GEE computation service enables users to select data with an import function, then process with a few lines of codes, with the final output exported into a csv file for further analysis. Therefore, having enough storage space is no longer an issue, and labor is greatly reduced.

2. Raw MODIS images use a Sinusoidal (SIN) projection, which, in this project, requires a reprojection before being clipped by the polygon shapefile of the study area. A MODIS reprojection tool (MRT) is available (https://lpdaac.usgs.gov/tools/modis_reprojection_tool) to convert the MODIS image projection and format into more commonly-used types. However, when dealing with many images, this reprojection and format converting process could be labor intensive, but the GEE platform greatly reduces the time needed to complete this task. First, by entering latitude and longitude of four corners of the plot, I can identify the boundary of the plots and create one polygon geometry for each. Then the geometries can be imported as variables for later use. Second, The ReduceRegions function is designed to process data within a defined region, which refers to the geometries for my cases. By applying this function, I don't need to clip each image with a polygon, so reprojection and format conversion are not required either.
3. Since the plots are relatively small, carrying out a relatively precise estimation based on limit pixels, the VI value of each pixel is weighted by their area of intersection within the plot (Liang et al., 2011). The ee.Reducer.mean() function provided by the GEE platform calculates a regional average weighted by intersection areas between each pixel and geometry, which frees users from computing the weight of each pixel manually.

Finally, based on these requirements, the exported result is in a csv file with attributes including calendar day, day of year (DOY), mean NDVI, mean EVI, standard deviation of NDVI and standard deviation of EVI.

The "DayofYear" column of the table is computed by the average day of year when the image is acquired. Therefore, the DOY value of the last record in an annual time series might be

invalid. For example, in 2000 for the northern plot, the penultimate day of year was 337, while the last day of the year is 202. That's because in the last row, some pixel data were acquired in the last several days of 2000, while the other data were acquired in the first days of 2001. As a result, the average day of year is unusually small, and the standard deviation is as great as 170.

To get a reliable DOY, I selected 16 evenly-distributed points in each plot and extracted their data into separate files. The GEE platform will return the data of pixels covering the points of interest. Then the pixel data acquired at the end of the year will be used to replace the invalid DOY values in the multi-pixel average files. In the previous example, the day of year value "202" will be replaced by "362".

b. Two different data processing methods before applying a model are required

The original data processing method is to put the raw data directly into the logistic model for regression analysis. Before processing the regression, initial parameter values should be identified for iteration. The output of the estimated parameters is sensitive to the initial input. To improve the efficiency of logistic regression model, two options were tested to manipulate the data before applying the model.

The first option is to use VI raw data directly for analysis, while the second option is to normalize the VI values following equation (1) as described in White 1997:

$$VI_{ratio} = \frac{VI - VI_{min}}{VI_{max} - VI_{min}} \quad (1)$$

The normalized VI value ranges between 0 and 1, so the minimum and maximum of VI time series are fixed. As a result, the regression model is simplified since fewer parameters are estimated. Furthermore, the uncertainty caused by the parameters is reduced.

In this project, original raw data and normalized data are applied to the regression model respectively, using twenty years of autumn data (1997-2017) used. The goodness of fit of the logistic model for these two options are compared using paired-sample T tests. If a significant difference is found ($P<0.05$), the option with higher goodness of fit will be selected for further analysis. Otherwise, if neither of these two methods is higher than the other one, the simplest one, which is the normalized data, will be chosen.

c. Applying two-section logistic models to derive SOA, MOA and EOA

The VI time series are dissected into two sections, the increasing section during spring and the decreasing section during autumn. Division of these two periods is identified as the corresponding date of year (DOY) when the minimum root-mean-square error (RMSE) value is found. In the original raw data, for the decreasing autumn section, a logistic-regression model is applied following equation (2), where *t* is time in days, *y(t)* is the VI value at time *t*, *a* and *b* are fitting parameters, and *c* + *d* is the maximum VI value (Zhang et al., 2003).

$$y(t) = \frac{c}{1 + e^{a+bt}} + d \tag{2}$$

Then the rate of change of curvature (CR) could be computed from equation (3), where $z = e^{a+bt}$,

$$CR = b^3 cz \left\{ \frac{3z(1-z)(1+z)^3\left[2(1+z)^3 + b^2c^2z\right]}{\left[(1+z)^4 + (bcz)^2\right]^{\frac{5}{2}}} - \frac{(1+z)^2(1+2z-5z^2)}{\left[(1+z)^4 + (bcz)^2\right]^{\frac{3}{2}}} \right\} \tag{3}$$

The DOY shows two minimum CR values in the decreasing section which represent the date of the start of autumn (SOA) and end of autumn (EOA), while the DOY corresponding to the maximum CR value represents the middle of autumn (MOA).

In normalized data, c and d are replaced by 1 and 0 respectively, which simplifies equation (2) and equation (3) into equations (4) and (5):

$$y(t) = \frac{1}{1 + e^{a+bt}} \tag{4}$$

$$CR = b^3 z \left\{ \frac{3z(1-z)(1+z^3)[2(1+z)^3 + b^2 z]}{[(1+z^4) + (bz)^2]^{\frac{5}{2}}} - \frac{(1+z)^2(1+2z-5z^2)}{[(1+z)^4 + (bz)^2]^{\frac{3}{2}}} \right\} \tag{5}$$

4.2.3 Deriving carbon flux phenology

a. Data acquiring and pre-processing

Carbon flux data for Park Fall can be downloaded from the AmeriFlux website. The data include hourly-interval raw and gap-filled records. In this project, only daytime records reflecting productivity were selected for processing since nighttime GPP is supposed to be zero and nighttime NEE tends to show the intensity of night respiration. Daytime is defined by the time of sunrise and sunset, which can be computed based on latitude of the carbon tower and day of year. Records are removed if day length is shorter than eight hours. However, no day length is shorter than eight hours in the study area, so all records are kept. Then all daytime records within a day are averaged to get the daily average NEE and GPP.

b. Fitting model deriving phenology based on carbon flux indices

In this project, a double-logistic function is applied to derive three inflection points during autumn: start of autumn (SOA), middle of autumn (MOA) and end of autumn (EOA). The function is described as equation (6), which originates from the double logistic function in Fisher (2006) and the two-section logistic model in Zhang et al. (2003).

$$y(t) = a + \frac{d}{1 + e^{ct+b}} - \frac{g}{1 + e^{ft+e}} \quad (6)$$

Where *y(t)* is the carbon flux indices value at time *t*, *a*, *b*, *c*, *d*, *e*, *f*, *g* are fitting parameters (*b*, *c*, and *d* are spring parameters while *e*, *f*, and *g* are fall parameters). Different from satellite data, carbon flux data are abundant but noisy. Therefore, *a*, *d*, and *g* are not set by the minimum and amplitude of carbon flux variation, although these are still their physical meanings. Instead, all parameters are estimated by non-liner regression.

Similar to satellite time series processing, carbon flux indices are normalized using equation (7) and equation (8).

$$NEE_{nor} = \frac{NEE - NEE_{max}}{NEE_{max} - NEE_{min}} \quad (7)$$

$$GPP_{nor} = \frac{GPP - GPP_{min}}{GPP_{max} - GPP_{min}} \quad (8)$$

Where NEE_{nor} and GPP_{nor} represent normalized NEE and GPP, and range between -1 to 0 and 0 to 1 respectively. Therefore, the double-logistic function is simplified into equation (9):

$$y(t) = \frac{1}{1 + e^{ct+b}} - \frac{1}{1 + e^{ft+e}} \quad (9)$$

Twenty-year time series are regressed for both original function (6) and simplified function (9), then goodness of fit are compared by paired-sample T tests. Subsequently, the option with either significantly higher accuracy ($P<0.05$) or simplicity (normalized data) will be selected to derive SOA, MOA and EOA.

Based on the algorithm developed by Zhang et al. (2003), transition dates are derived from the minimum and maximum values of change of curvature (10):

$$CR = [\frac{|y''(t)|}{(1+y'(t)^2)^{\frac{3}{2}}}]' \tag{10}$$

Where the two maximum values represent for SOA and EOA respectively, and the minimum represents MOA.

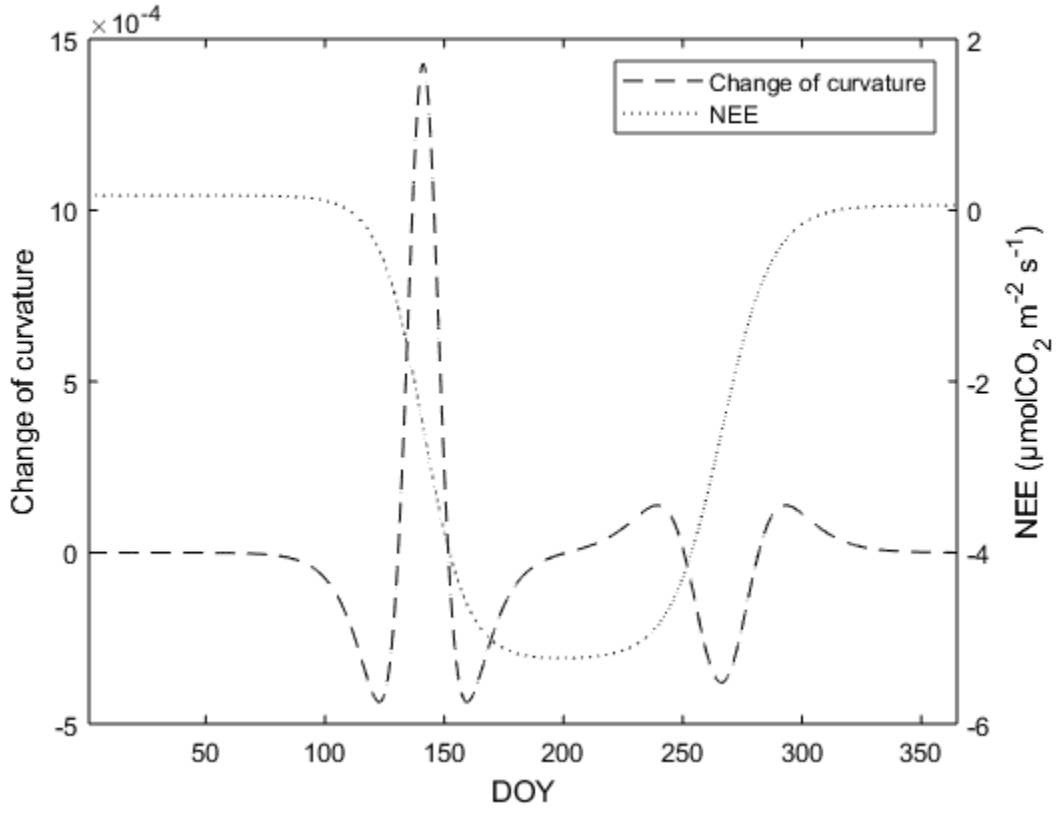

Figure 3. An example of annual NEE and change of curvature (CR) variation.

Source data: unnormalized NEE time series in 2016.

4.2.4 Comparison among three measurements

Satellite data are useful when they provide researchers with possibilities to monitor phenology where no field data are available. That advantage also facilities phenological studies at continental or global scales. However, the reliability of satellite data is a debatable issue. First, orbit errors and cloud cover can affect the accuracy of satellite data. Second, the monitoring frequency is restricted by the temporal resolution of satellites (Sellers et al., 1992). Furthermore, the accuracy of satellite-derived phenology varies with attributes of the model themselves (Beck et al., 2006; White et al., 2014).

As for carbon flux measurements, NEE is an indicator of the carbon exchange rate between an ecosystem and atmosphere, while an ecosystem is composed of trees, grass, animals, soil bacteria, and other lifeforms. GPP is the productivity of all producers, although deciduous forest plays the predominant role in this study area. Therefore, NEE and GPP values are contributed by living activities of various organisms, but not only those measured in this study. Thus, the accuracy of estimating forest phenology based on NEE and GPP needs to be clarified.

For each measurement, a comparison with ground-based reference data is conducted for available years. When no field data is available, comparison between satellite data and carbon flux indices is conducted. The comparison can be classified into two types: comparison of phenology transition dates and comparison of senescence rate parameters.

a. Comparison of phenology transition dates

For each measurement, SOA, MOA and EOA are computed. In the years when field data is available, root mean square error (RMSE) and bias (Soudani et al., 2008) between field observation and other measurements are calculated for each transition date.

$$Bias = \frac{\sum_n^i (M_i - O_i)}{n} \quad (11)$$

Where M_i is the transition date for a certain measurement (field data, satellite data or carbon flux indices), O_i is the transition date of observation, n is the pair of comparisons. Apart from that, for each year, the DOY of each seasonal marker is put into field-derived fitting model to get a corresponding field phenology.

When field data are unavailable, for each seasonal marker, the RMSE and bias between satellite data and carbon flux data is calculated.

4.2.5 Comparison of parameters

Logistic regression is non-liner regression, so simply doing linear correlations among the logistic fitted curves of different approaches might not show their mechanistic relationships. However, logistic models are exponentially linear models, which can be converted into a linear form using logarithms. The extracted linear part in a two-section logistic model includes only two parameters (a and b), each of which has a biological meaning (Zhang, 2015). In a two-section logistic model (equation (2)), the absolute value of parameter b is the rate of vegetation growth or senescence, while the absolute value of a/b is the peak of growth or senescence, which equals to MOS or MOA. Similarly, in double-logistic functions, the absolute value of parameter c and f are the rate of vegetation growth or senescence, while the absolute value of b/c and e/f are the peak of growth or senescence (Beck et al., 2006). Therefore, the linear correlation of linear parameters derived from different approaches shows the difference and relationship of these approaches in measuring the rate and peak of vegetation growth and senescence.

For satellite data and carbon data, linear correlation of senescence rate parameters is conducted. In the linear regression model, the constant is manually set as zero since an intercept doesn't have any physical meaning while the slope shows how many times the rate derived from one approach is compared to another approach. RMSE is used to evaluate the quality of model instead of R square because the latter in not applicable in a non-constant regression model. Similarly, the significance (P value) for the model is derived from T test rather than F test for the same constant issue.

In the years with field data, RMSE and bias are used for rate parameters from three approaches rather than linear regression, considering the field data covers up to three years.

The peak of the senescence parameter, which is a/b, b/c or e/f depending on the case, derived from each approach, as discussed earlier, is the same as MOA. Therefore, the comparison is accomplished in an earlier section and is not analyzed separately.

5. Results

5.1 The influence of normalization

5.1.1 Satellite data

For the raw and normalized satellite time series, neither parameters nor R square values show significant differences (Table 4). Especially for parameter a in the south site, values are the same within the first few decimals, so the standard error of difference is taken to be 0. A T value cannot be computed under this situation, explaining the N/A value in Table 4. The similarity in parameters suggests the fitted curves derived from raw and normalized datasets are nearly the same and perform equally effectively for estimating phenology transition dates. Consequently, normalization doesn't have a significant impact on the quality of time series. Considering normalization simplifies the fitting model, normalized datasets are used to derive satellite-based phenology transition dates.

Table 4 Comparison of parameters and goodness of fit for raw and normalized datasets

		a		b		R^2	
		mean	P value	mean	P value	mean	P value
north	EVI	0.078	0.269	-20.297	0.435	0.970	0.257
	EVI_{nor}	0.078		-20.297		0.969	
	NDVI	0.219	0.331	-58.427	0.071	0.981	0.189
	$NDVI_{nor}$	0.219		-58.427		0.984	
south	EVI	0.065	N/A	-16.758	0.331	0.973	0.498
	EVI_{nor}	0.065		-16.793		0.974	
	NDVI	0.190	N/A	-50.484	0.042	0.962	0.720
	$NDVI_{nor}$	0.190		-50.622		0.963	

5.1.2 Carbon data

For both GPP and NEE, the goodness of fit for normalized datasets is significantly lower than for raw datasets. For GPP, dataset mean R square slightly decreases by 0.006 after normalization, while the difference is 0.102 for normalized NEE. This result suggests normalization has less impact on GPP than on NEE, although even this small impact is significant in terms of data accuracy (Table 5).

Table 5. Comparison of goodness of fit for raw and normalized datasets

Variables	GPP	GPP_{nor}	NEE	NEE_{nor}
Mean	0.942	0.936	0.827	0.725
P value	0.000		0.000	

To further investigate raw and normalized dataset differences, the model fitted curve and corresponding change of curvature are provided in Figure 4. For both GPP and NEE, normalized curves show different shapes, which are revealed by their change of curvature. For modeled NEE, shape differences are obvious in both spring and autumn. For raw datasets, both decreasing and increasing sections show three transition points. However, for normalized datasets, there are only two transition points throughout the year (Figure 4 (a), (b)). Although Figure 4 is based on 2016 data, similar patterns occur in all available years. From autumn 1997 to 2016, among 18 available time series, three years have two transitions (1997, 1999 and 2006) while the other years only have one transition. However, all years have three transitions in raw time series (except 2015, with only one transition). Therefore, it will be problematic to use normalized NEE

to derive autumn phenology transition dates. As for modeled GPP in 2016, shape differences are not obvious in spring, as both raw and normalized datasets show three transition points on change of curvature. However, in autumn, although both raw GPP time series and normalized time series produce three transition points, the transitions in raw time series are defined by two maximum and one minimum while in the normalized time series they are defined by one maximum and two minimums (Figure 4 (c), (d)). This indicates the shape of fitted curve are different despite the number of transition point staying the same. Among the 18 available time series, six years produce three valid transitions (1997, 1998, 1999, 2009, 2014, 2016), seven years produce two transitions (2000, 2001, 2002, 2003, 2004, 2012, 2015) and the others produce only one transition. Therefore, although normalization has a weaker impact on GPP compared with NEE, it will still be problematic to apply normalized GPP in deriving phenology transition dates. Thus, for both NEE and GPP, raw time series are used for further analysis.

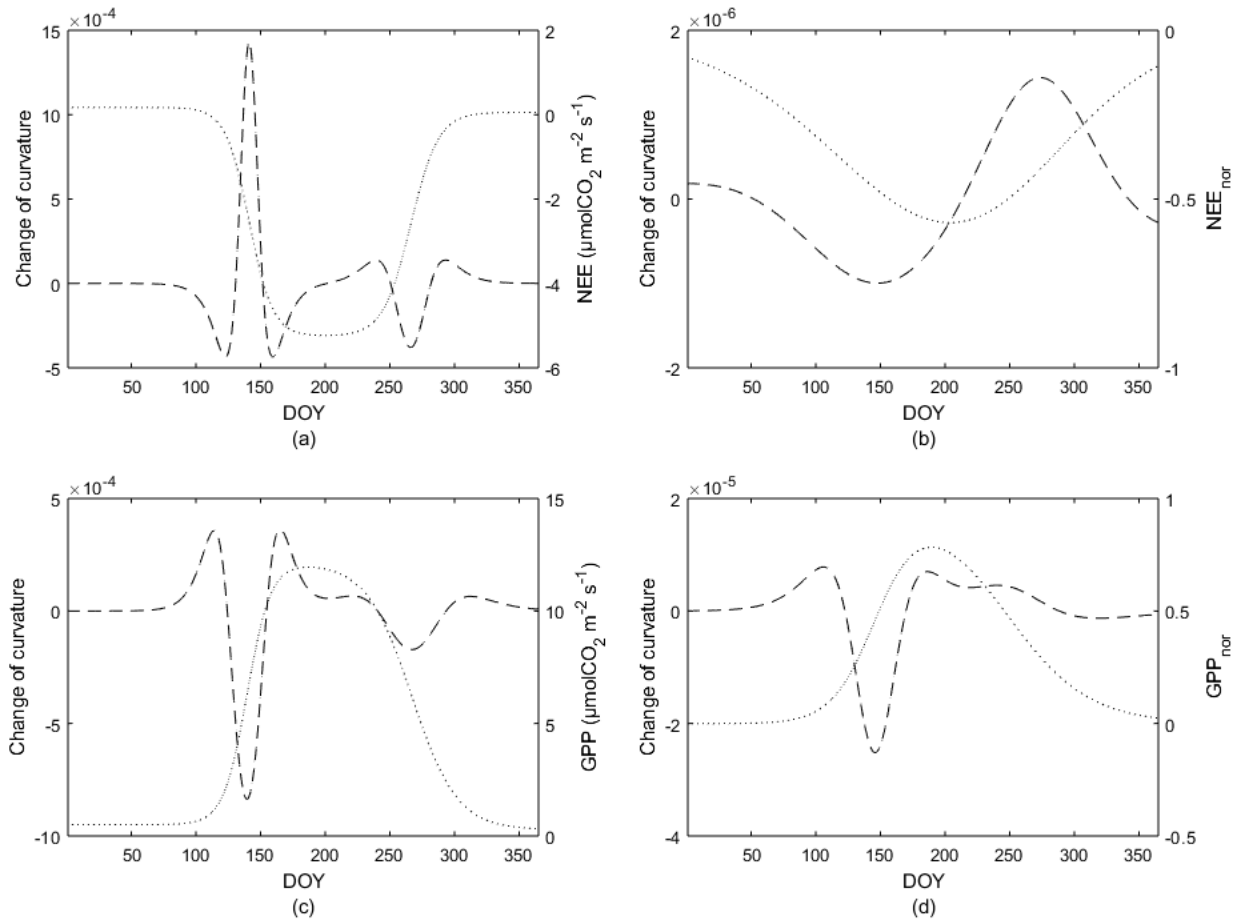

Figure 4. Modeled carbon flux time series and change of curvature.

The dotted lines show carbon flux indices (scale on right axis), and dashed lines show change of curvature (scale on left axis). (a) is modeled NEE raw time series and its change of curvature in 2016, and (b) is for normalized NEE time series in 2016. (c) represents for GPP raw time series in 2016 while (d) represents for normalized GPP time series in the same year.

5.2 Year-by-year comparison with field data

5.2.1 Transition dates

For the north site, start of autumn (SOA) dates derived from all four datasets are earlier than the first transition of leaf coloration and leaf fall. Among them, NEE shows the most advanced gap (as much as 78 days from leaf coloration and 83 days from leaf fall). For

normalized satellite data, EVI has a larger bias than NDVI. As for middle of autumn (MOA), all four indirect measurements are still earlier than the second transition of leaf coloration and leaf fall, but all the absolute bias errors are smaller than for SOA. The gap between indirect approaches and observation shows the order of NEE> GPP>EVI> NDVI, which is consistent with the order found in SOA. As for end of autumn (EOA), NEE derived EOA is eight days earlier than leaf coloration while 16 days earlier than leaf fall. Normalized EVI results in later EOA than leaf coloration while it predicts leaf fall perfectly. On the contrary, normalized NDVI always results in earlier EOA than leaf coloration. The bias error between indirect measurements and observations is further reduced at the end of senescence, indicating the physiological stage of deciduous trees, ground spectral feature and ecosystem activity intensity become more consistent.

For the south site (like north site), start of autumn (SOA) and middle of autumn (MOA) derived from the four approaches are all earlier than both leaf coloration and leaf fall. For both SOA and MOA, (and both leaf coloration and leaf fall stage), the order of bias error follows the same pattern as for the north site, which is NEE>EVI>NDVI. However, a GPP bias error is available for the south site. For SOA, the absolute bias of GPP is smaller than that of normalized EVI. The absolute bias error between GPP and leaf coloration or leaf fall stage is lower than EVI by 24 days. For MOA, GPP bias error still falls between normalized EVI and normalized NDVI. GPP bias errors are four days less than EVI for the leaf coloration and three days less for the leaf fall stage. As for end of autumn, the smallest absolute bias errors from leaf coloration and leaf fall are in NEE while the greatest are in GPP which are as much as 26 days later than leaf coloration and 21 days later than leaf fall. For EVI and NEE, the gap from both leaf coloration

and leaf fall becomes smaller with phenological progression, while this trend is not found in GPP and NDVI.

Table 6. Average bias error of transition dates

		Leaf Coloration			Leaf Fall		
	Site	Start	Middle	End	Start	Middle	End
EVI_{nor}	N	-31	-11	9	-36	-14	0
	S	-52	-20	13	-56	-24	7
$NDVI_{nor}$	N	-9	-7	-5	-15	-9	-14
	S	-4	-7	-6	-12	-11	-12
NEE	N	-78	-49	-8	-83	-56	-16
	S	-66	-39	4	-71	-44	-1
GPP	N	N/A	-30	N/A	N/A	-37	N/A
	S	-28	-16	26	-32	-21	21

For the north site, field data are available for 2010 and 2012. Since carbon data in 2010 is unavailable, the carbon bias error is based only on data from 2012. In autumn 2012, GPP model provides only one output, which is taken as MOA, then the comparison for the other two transition dates are inapplicable. For the south site, field data are available for 2010, 2012, and 2013, so carbon bias error is computed from the average of 2010 and 2013 data.

5.2.2 Senescence rate

Table 7 shows the senescence rate derived from field observation and indirect approaches. For the south site, average rate based on normalized NDVI is faster than that of leaf coloration and leaf fall. However, under all the other situations, the average rate derived from indirect approaches are slower than either leaf coloration or leaf fall. The reliability of each approach can be evaluated by the difference between the computed ratio and one--the shorter

distance representing better estimation. Thus, the reliability of EVI derived leaf coloration and leaf fall rate for the north site is better than for the south site. Meanwhile, NDVI, NEE and GPP perform better in estimating south site leaf coloration and leaf fall rate than for the north site. In the north site, reliability of approaches in estimating both leaf coloration and leaf fall rate follows the order of NDVI> EVI> NEE and GPP. For the south site, the reliability of approaches follows the order of NDVI> EVI> GPP > NEE. In both sites, satellite data performs better than carbon data, while for satellite data, NDVI performs better than EVI. In addition, in both sites, the reliability of NEE and GPP are similar, with ratio varying between 9.88 to 9.95 for north leaf coloration, and 7.76 to 9.32 for south leaf coloration; for leaf fall, the ratio varies between 9.11 to 9.17 in north site and between 7.25 to 8.49 in south site. However, the reliability order of these two indices could switch, which probably depends on the community composition of these two plots.

Notably, the reliability of approaches in estimating senescence rate can't solely determine their accuracy in studying phenology. In fact, rate only determines the distance between start and end of autumn, which is the length of senescence. The midpoint of senescence, which is also MOA (discussed in last section), determines the time of year of senescence. To thoroughly compare different datasets, considering both senescence rate and midpoint time is necessary. In Table 6, NDVI derived MOA for both sites shows smaller bias error from the midpoint of leaf coloration and leaf fall than the other approaches. Together with the higher reliability in estimating senescence rate parameter (Table 7), it's reasonable to conclude that the NDVI time series can more accurately describe both leaf coloration and leaf fall than the other datasets. As for EVI, NEE and GPP, (in both the north and south sites), both leaf coloration and leaf fall stages show the greatest midpoint bias errors for NEE, while the bias order of EVI and GPP are

not fixed. Conversely, the senescence rate difference between field data and either NEE or GPP is greater than EVI, while only small differences exist between the former two. Therefore, NEE can be treated as the least reliable approach with slightly lower performance than EVI and GPP, while the accuracy order of EVI and GPP is hard to determine.

In conclusion, the accuracy of the four datasets can be summarized as: NDVI is the most reliable one in terms of senescence rate and senescence time of the year and the least reliable one is NEE. The accuracy of EVI and GPP are variable and might be altered by the properties of the plots. However, EVI performs better in estimating senescence rate than GPP.

Table 7. Senescence rate parameter for each approach from 2010 to 2013

Year	Site	EVI_{nor}	$NDVI_{nor}$	NEE	GPP	LC	LF
2010	North	0.13	0.32	N/A	N/A	0.43	0.28
	South	0.06	0.18			0.41	0.27
2012	North	0.07	0.37	0.05	0.05	0.50	0.58
	South	0.06	0.24			0.45	0.55
2013	South	0.05	0.83	0.04	0.05	0.36	0.29
Average ratio to field observation							
LC	North	4.62	1.35	9.88	9.95	-	-
	South	6.98	0.97	9.32	7.76	-	-
LF	North	4.26	1.24	9.11	9.17	-	-
	South	6.35	0.88	8.49	7.25	-	-

LC represent for leaf coloration and LF represent for leaf fall.

5.3 Long-term comparison between satellite data and carbon data

5.3.1 Transition dates

Since long-term field observations are unavailable, a potential compensation for this is to use available observation data as a proxy long-term record. This approach assumes that observation record-available years are not abnormal over the long-term. To test this assumption, the z value of start, middle and end of autumn derived from normalized EVI, normalized NDVI, NEE and GPP were computed. If a z value exceeds three, then the corresponding record is treated as an outlier. Results show for all four approaches and three transition dates, the z values in 2010, 2012 and 2013 are smaller than three, suggesting the transition dates in these three years are normal and consistent within long-term records (Appendix A, B and C). Therefore, the average of observation transition dates in these years (2010 and 2012 for north site and 2010, 2012 and 2013 for south site) are computed and taken as representative of a long-term field record which is then compared with transition dates computed from long-term indirect approaches.

The phenological transition dates derived from normalized EVI, normalized NDVI, NEE and GPP during 1997 to 2017 were compared. The available field data are used as reference lines in Figure 5. For start of autumn, for both the north and south sites, all four indirect approaches show an earlier average start than either leaf coloration or leaf fall starts. In the north site, bias error from both leaf coloration and leaf fall stages (shown by the distance between mean of each approach and the two observation-based reference lines), is greatest for NEE and smallest for NDVI. The bias error based on EVI, NEE and GPP varies within seven days (36 to 43 days for leaf coloration stage and 41 to 47 days for leaf fall stage) while the bias error for NDVI is lower (9 days for leaf coloration stage and 14 days for leaf fall stage). In the south site, greatest bias

error is for EVI, which exceeds NEE bias by three days and GPP bias by nine days. Meanwhile, the smallest bias error is still from NDVI (Figure 5 (a), (b)). For middle of autumn, all eight means from the two sites are earlier than the second transition of leaf coloration and leaf fall. For both sites, bias error is greatest for NEE and smallest for NDVI. In the north site, NEE bias error is ten days larger than EVI and nine days larger than GPP. In the south site, NEE bias error is five days larger than EVI and ten days larger than GPP (Figure 5 (c), (d)). For end of autumn (except for the mean derived from NDVI overlapping with the third transition of leaf fall in south site and being earlier than that transition by one day in north site), all the other six means from two sites are later than the third transition of leaf coloration and leaf fall. In both sites, the bias error is smallest for NDVI, and GPP biases are the largest, exceeding EVI bias by four days in the north site and three days in the south site; while exceeding NEE bias by six days in both sites (Figure 5 (e), (f)).

In general, NDVI shows the minimum bias error with leaf coloration and leaf fall in all stages and both sites, while the maximum bias error can come from either NEE or GPP. The bias derived from EVI, NEE and GPP differ by up to ten days (north site middle of autumn and leaf fall stage, between EVI and NEE).

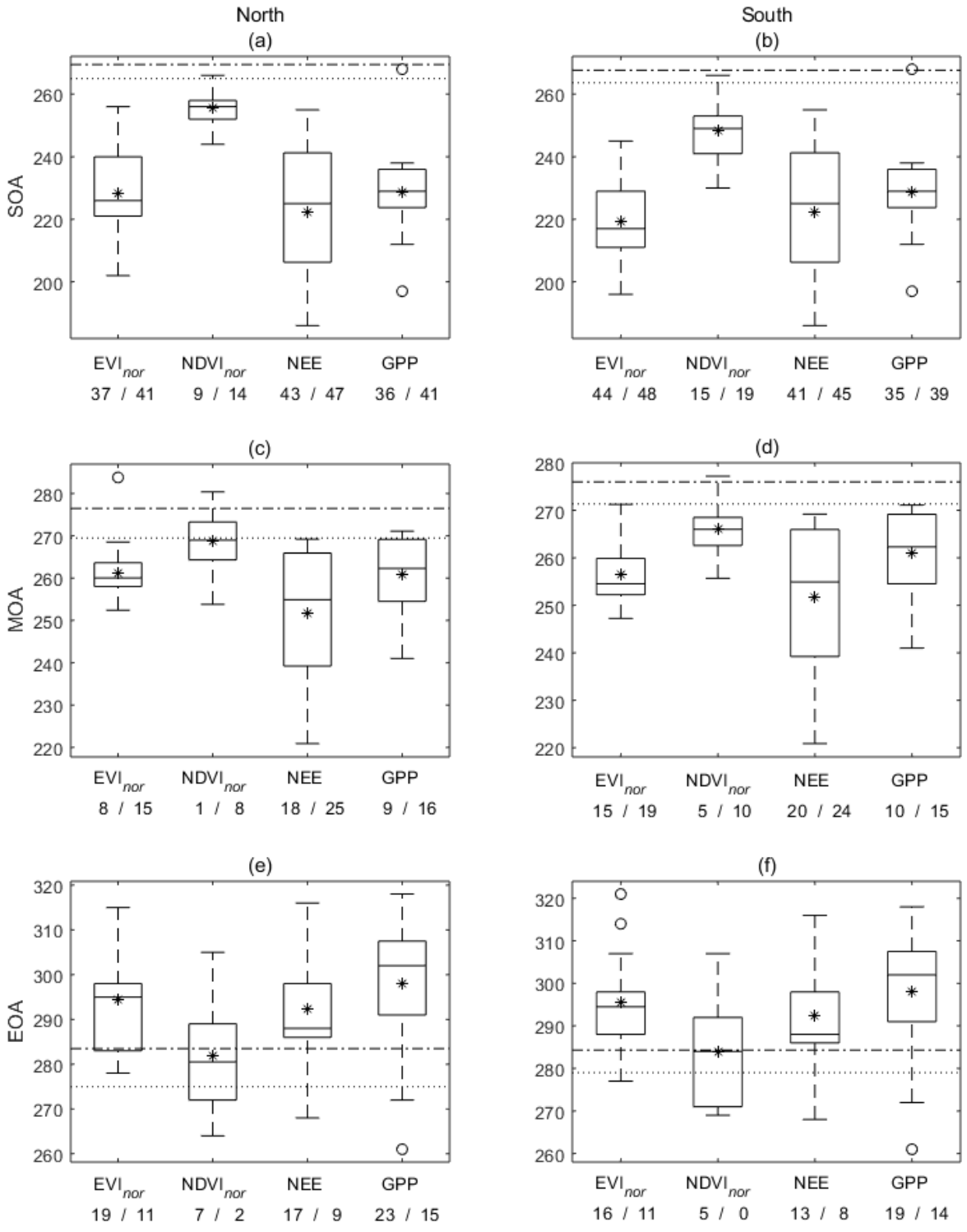

Figure 5. SOA, MOA and EOA are start of autumn, middle of autumn and end of autumn respectively.

Dot-dash lines show the first, second and third transition of leaf coloration, while the dotted lines show the first, second and third transition of leaf fall. Data are from the average of all field data available years at each site. The star in each box represents mean values and hollow dots represent outliners. Numbers below each label show bias errors between mean values of each approach and leaf coloration/leaf fall stage. Although bias errors are calculated using mean dates of one approach minus leaf coloration or leaf fall date (which results in both positive and negative numbers), the absolute value is used for convenience.

5.3.2 Progression rate

Like transition dates, the z values of long-term progression rate for the four datasets were computed. Result show the south site NDVI derived progression rate in 2013 is an outliner (z value = 3.62). However, since z values derived from the other three approaches in that year are relatively small (-0.49 for EVI, -0.80 for NEE, 0.25 for GPP), this abnormal large value in NDVI is not enough to judge 2013 as an abnormal year (Appendix D). Therefore, the field record in 2013 is still treated as a representative of long-term observations and utilized to generate mean leaf coloration and leaf fall rate.

Different from year-to-year comparison, long-term comparison suggests all four indirect approaches underestimate leaf coloration and leaf fall rate at both sites. However, indirect approaches still perform better in estimating leaf coloration rate than leaf fall rate. Moreover, NDVI remains the highest reliability for both sites and stages. Conversely, the reliability orders of EVI, NEE and GPP differ between sites. For both leaf coloration and leaf fall stage, in the north site, the reliability order is NDVI> EVI> GPP> NEE, while in the south site, the order is NDVI> GPP> EVI> NEE. Although the orders are inconsistent, the difference between long-term EVI, NEE and GPP decrease rate is relatively small. Specifically, for the north site, the ratio varies between 5.97 to 7.23 in estimating leaf coloration and 5.50 to 6.67 in estimating leaf

fall; for the south site, the ratio varies between 5.56 to 6.30 in estimating leaf coloration and 5.07 to 5.74 in estimating leaf fall (Table 8).

Table 8. Progression rate ratio between field data and indirect approaches

Year	Site	EVI_{nor}	$NDVI_{nor}$	NEE	GPP
LC	North	5.97	2.11	7.23	6.38
	South	5.50	1.95	6.67	5.89
LF	North	6.19	2.12	6.30	5.56
	South	5.64	1.93	5.74	5.07

LC represent for leaf coloration and LF represent for leaf fall.

Apart from their reliability in estimating leaf coloration and leaf fall rate, when not considering field data, the linear relationships between progression rate derived from four indirect approaches can be computed. Over the long-term, normalized EVI rate is slower than normalized NDVI rate. Specifically, in the north site, EVI rate is 30.3% of NDVI rate, while in the south site, EVI rate is 34.1% of south rate. The rate derived from EVI and carbon measurements are close, where EVI rate is 1.015 times as much as NEE rate in the north site, while 0.886 times as much of NEE rate in the south site. EVI rate is slightly faster than GPP rate, being 0.246 times higher in the north site and 0.142 times higher in the south site. Conversely, NDVI rate is much faster than the two carbon measurements. Markedly, NDVI rate is 2.053 to 1.159 times faster than NEE and 2.316 to 2.551 times faster than GPP. The rate of NEE and GPP are nearly the same with a ratio of 1.021. All these regressions are very significant ($P<0.01$), and RMSE varies within 0.021 and 0.138, suggesting stable relationships with low error levels.

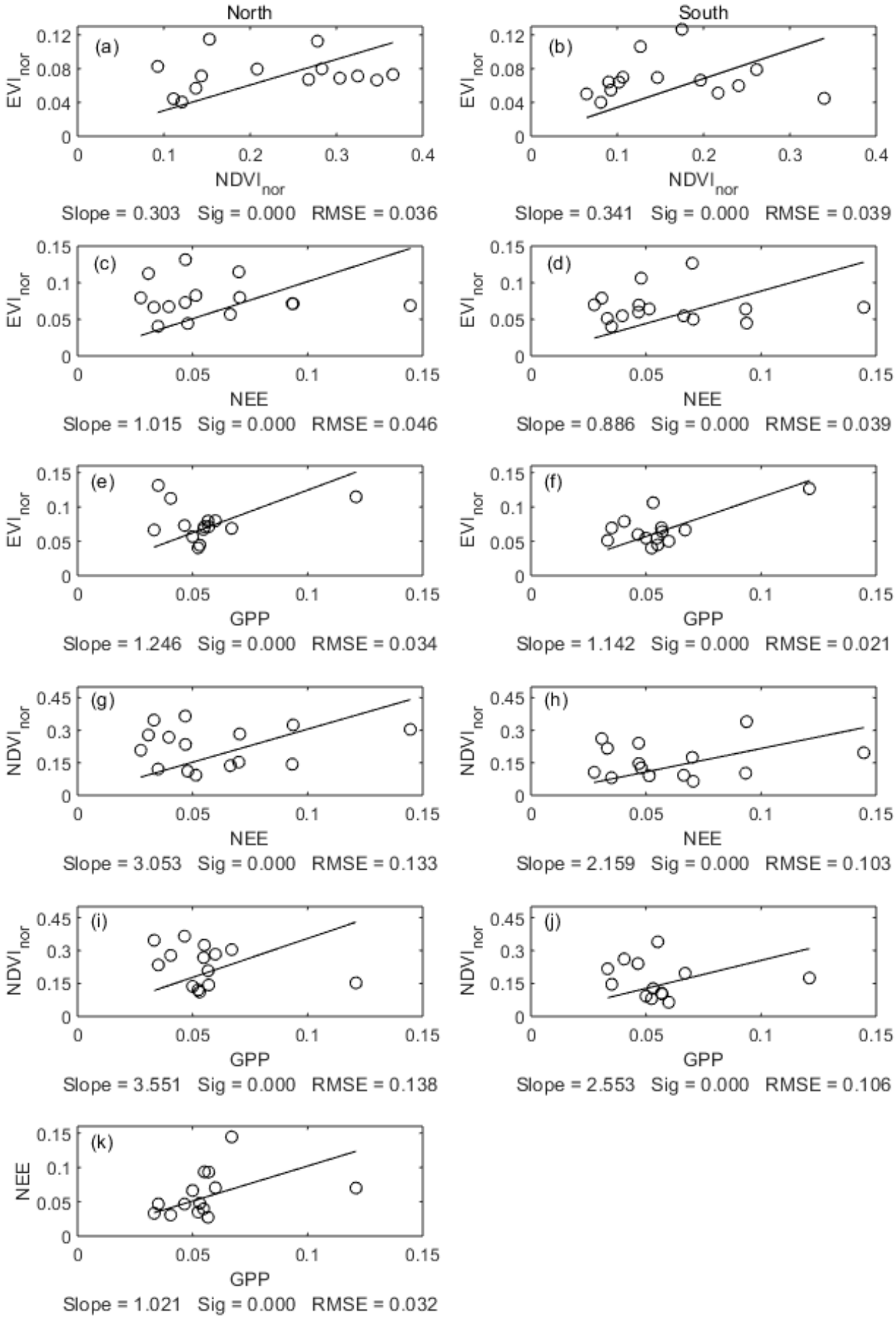
North
South
(a)
(b)
(c)
(d)
(e)
(f)
(g)
(h)
(i)
(j)
(k)
EVI_nor
NDVI_nor
NEE
GPP
Slope = 0.303 Sig = 0.000 RMSE = 0.036
Slope = 0.341 Sig = 0.000 RMSE = 0.039
Slope = 1.015 Sig = 0.000 RMSE = 0.046
Slope = 0.886 Sig = 0.000 RMSE = 0.039
Slope = 1.246 Sig = 0.000 RMSE = 0.034
Slope = 1.142 Sig = 0.000 RMSE = 0.021
Slope = 3.053 Sig = 0.000 RMSE = 0.133
Slope = 2.159 Sig = 0.000 RMSE = 0.103
Slope = 3.551 Sig = 0.000 RMSE = 0.138
Slope = 2.553 Sig = 0.000 RMSE = 0.106
Slope = 1.021 Sig = 0.000 RMSE = 0.032

Figure 6. The linear relationships of progression rate derived from four indirect measurements (normalized NDVI, normalized EVI, NEE and GPP).

For either site, two of these four approaches are selected, and their rate parameters are regressed. The intercept of each regression is set as zero, and the slope below each subplot represents for the numerical relationship between the rate of the regressed two datasets. If slope is greater than one, then the rate derived from the vertical axis dataset is faster than that of the horizontal axis dataset, and vice versa. Significance and RMSE show the quality of regressions. Since the same NEE and GPP dataset are shared by north and south site, only one regression is computed.

From these linear regressions, the order of long-term progression rate can be described as: NEE≈ GPP≈ EVI< NDVI. However, the reliability of indirect approaches to reflect canopy change is also determined by bias errors between their midpoint and second transition of leaf coloration and leaf fall. This bias is represented in Figure 5, where the bias is smallest in NDVI, largest in NEE while the order of EVI and GPP differ between plots. NDVI decrease rate is closest to canopy autumn progression although it's still slower. At the same time, the midpoint of NDVI decrease is closest to the midpoint of leaf coloration and leaf fall. Integrating middle of autumn and autumn progression rate, it's reasonable to conclude NDVI has the highest temporal consistency with canopy change.

The midpoints of all the other three approaches are a few days later than the second transition of leaf coloration and leaf fall, showing delayed development of autumn canopy phenology. Meanwhile, their decrease rates are all slower than leaf coloration and leaf fall, resulting in earlier start of autumn, later end of autumn and longer timespan than observed canopy autumn progression duration. Considering their close decrease rate and flexible bias order, the reliability of EVI, NEE and GPP are similar in terms of estimating observed canopy phenology, which are all lower than that of NDVI. In addition, their similarity in terms of

sensitivity to canopy change indicates higher accuracy in estimating carbon flux indices from EVI than NDVI in a forest ecosystem.

In general, the conclusion from year-to-year comparisons is reinforced: NDVI shows the highest accuracy in estimating observed phenology while the order of the other three approaches is not fixed.

6. Discussion

6.1 Issue with incomplete time series

Ideally, the intersection of curves and phenology in the leaf coloration stage would be 800, representing leaf coloration having not started in an earlier day of year (DOY). However, the intersections are higher than 800 in north site years 2010 and 2012, as well as for south site years 2010 and 2012. This could be a result of the late start of observations. When observation started in the north site, DOY was 263 in 2010 and 260 in 2012; for the south site, DOY was 265 in 2010 and 262 in 2012. Further, most species had already entered leaf coloration stage. Specifically, for the north site, except for Tamarack in 2010 and Basswood in 2012, the population phenology of all the other species are higher than 800. For the south site, at the time when observation started, the population phenology for all species are greater than 800. Following population phenology, the first record of landscape phenology was higher than 800. Therefore, for these four time-series, the leaf coloration values earlier than the first day of observations overestimate the true leaf coloration stage. However, this problem disappears after the observations start, which means values occurring later than the first day of observation are reliable. A similar problem exists in 2013, in the south site, when observations ends before full leaf coloration and full leaf fall are observed on every tree. By the end of observation, most of the species have shown full leaf coloration and full leaf fall except for S. Alder. This matches with the report of Alder leaves staying green (and attached) until early November, and finally being killed by frost rather than naturally falling (Koike et al., 2001). The late phenology of S. Alder, when reflected by landscape phenology, causes leaf coloration and leaf fall phenology ending before full leaf coloration and full leaf fall. This would lead to the underestimation of leaf coloration and leaf fall proportion at the end of growing season.

6.2 Field observation and satellite data

6.2.1 Field observation corresponds with satellite phenology transition dates

For EVI, in the north site, when EVI detects increase in progression rate, the ground leaf coloration proportion is 8% in 2010 and 5% in 2012. In the south site, the first transitions detected by EVI correspond with 14% of leaf coloration in 2010, 5% of leaf coloration in 2012 and 0% of leaf coloration in 2013. However, considering the issue with late start of observations, the true leaf coloration stage is better reflected by the slope of transition dates, which are quite flat in all five situations, indicating the leaf coloration haven't started yet. EVI derived middle of autumn (MOA), although later than start of autumn (SOA), still corresponds with a flat slope in all five situations. In the north site, in 2010, EVI derived MOA overlaps with the first transition of leaf coloration, when leaf coloration proportion is 19%; in 2012, EVI derived MOA corresponds with 5% of leaf coloration, but the flat slope still suggests the leaf coloration hasn't started. Similarly, in the south site, EVI derived MOA occurs earlier than the first transition of leaf coloration in all three years, with a flat slope suggesting the observed leaf coloration progress hasn't started. However, EVI derived end of autumn (EOA) occurs at the late phase of leaf coloration. In all five situations, EVI derived EOA occurs later than the third transition of leaf coloration, after full leaf coloration. The same phenomenon is found for leaf fall. Since leaf fall tends to be a few days later than leaf coloration, it's reasonable to find EVI derived SOA and MOA are earlier than the first transition of leaf fall, meaning EVI decreases during this period has a minimal relationship with leaf fall processes. In the north for year 2010, EOA derived from EVI is only one day ahead of the third transition of leaf fall, while in the other four situations, EOA are all later than full leaf fall. Consequently, the latter half of EVI decrease covers the time span of the leaf autumn progression, and leaf coloration and leaf fall are likely to causes this

decrease. However, judging by the fact that EVI stops decreasing a few days after full leaf coloration and full leaf fall, if not quite close to it, other signals in addition to deciduous leaf progression are also detected by EVI.

For NDVI, the order between satellite transition dates and field transition dates are not fixed. In 2010, for both the north and south sites, NDVI derived start of autumn (SOA) occurs before leaf coloration and leaf fall first transits. In the north site, the corresponding leaf coloration proportion is 9% while in the south site it's 14%; the proportions of leaf fall are 1% for both sites. The slopes are all flat. In 2012, SOA also occurs before the first transition of leaf coloration and leaf fall, corresponding with leaf coloration proportion of 5% and 7%; and leaf fall proportions 4% in both sites, where the slopes are also flat. In 2013, SOA is later than the first transition of leaf coloration and one day before the first transition of leaf fall, where the leaf coloration proportion is 10%, leaf fall proportion is 15% but slopes show increasing trends. Overall, SOA corresponds with low leaf coloration and leaf fall proportions and flat slopes. Similar to EVI results, SOA occurs when leaf coloration and leaf fall processes haven't been observed yet. However, compared with EVI, the differences between NDVI and the first transition of leaf coloration and leaf fall are smaller. Interestingly, middle of autumn (MOA) is quite close to the first transition of leaf coloration and leaf fall. Specifically, in terms of leaf coloration, for south site year 2010, NDVI derived MOA overlaps with the first transition of leaf coloration, while in north site year 2010, they differ by only one day. The differences in south site year 2010 is three days, while the difference between north site year 2012 and south site year 2013 are greater (both six days). In terms of the difference between NDVI derived MOA and the first transition of leaf fall, the differences vary between two to eleven days. In general, the first half of NDVI decrease occurs before leaf coloration and leaf fall starts, and when NDVI decrease

rate reaches its peak, leaf coloration and leaf fall either has just started accelerating or will accelerate shortly. NDVI derived EOA in all five situations occurs before the last transition of leaf coloration and leaf fall. In 2010, it's close to the last transition of leaf coloration, corresponding with 75% and 80% of leaf coloration in both sites. At that time, leaf fall proportion in the north site is 24% and 53% in south site. In 2012, end of autumn (EOA) corresponds with 20% of leaf coloration in the north site, which is earlier than the second transition of leaf coloration, while leaf fall hasn't started yet. In the south site, EOA corresponds with 41% and 7% of leaf coloration leaf fall proportion. In 2013, EOA occurs when leaf coloration proportion is 36% and the second leaf coloration transition is in one day. On the other hand, leaf fall proportion is 15% and the second transition is in five days. Summarizing these five situations, the second half of NDVI decrease corresponds with the early section of leaf coloration and leaf fall. The midpoint of NDVI decrease is close to the first transition of leaf coloration and leaf fall, suggesting NDVI decrease and leaf coloration process starts temporally overlap after NDVI reaches it midpoint. Therefore, leaf coloration and leaf fall may play an important role in the second half of NDVI decrease. However, in all five situations, NDVI stops decreasing when leaf coloration and leaf fall is still in process, suggesting NDVI loses the signal of canopy change near the halfway point of leaf progression.

6.2.2 The reason of mismatch between field observation and satellite data

Both EVI and NDVI start to decrease before leaf coloration and leaf fall start, with half of EVI and NDVI decline having no overlap with observed leaf coloration and leaf fall duration. This mismatch can be caused by different leaf phenology between top-canopy and bottom-canopy. It is argued that canopy senescence pattern in autumn can be inner type or outer type. Leaves of an inner type canopy senesce from bottom to top, and vice versa (Koike, 1990). For

inner type canopies, the ground upwards-observation will detect earlier senescence than satellite downwards-observation, while ground observation will be later than satellite information for outer-type canopies. Maple is reported to be an outer-type species (Koike et al., 2001), which is the largest population proportion in the north site and second largest in the south site. This may cause earlier VI decrease than observed leaf senescence. However, the reports on inner-type and outer-type species are limited, with no information reported for Aspen, which is the largest population in the south site. It will be helpful to explore the canopy senescence pattern of more species to understand the difference between ground observation and satellite-based phenology. A possible way to do this could be utilizing PhenoCam network data. Compared with satellite data, PhenoCam images are not influenced by the atmosphere and clouds, providing near-surface digital information with better resolutions (http://explore.phenocam.us/). The fine resolution enables species-specific above-canopy analysis, which is suitable to category the canopy senescence pattern of different species. In addition, PhenoCam data are also used for comparison with satellite data (Richardson et al., 2007; Dragoni et al., 2011; Richardson et al., 2018).

The difference between EVI and NDVI is shown by the earlier start and later end of EVI time series. The earlier decrease of EVI could relate to its higher sensitivity for canopies with high leaf area indices (LAI). It is argued that NDVI is only sensitive to canopy change when LAI is less than 2. Once LAI progresses beyond this range, NDVI will saturate and stay stable during the middle of the growing season (Gamon et al., 1995; Motohka et al., 2010; Goswami et al., 2015), so the early leaf coloration and leaf fall will not be detected. EVI, in contrast, avoids this issue due to its overall lower values, and can detect canopy change in the early period of leaf progression when LAI values are higher (Huete et al., 2002).

Meanwhile, EVI and NDVI also differ at the end of growing season, when NDVI decrease stops halfway through leaf autumn progression, while EVI stops decreasing after full leaf coloration and full leaf fall, if not quite close to them. The reason NDVI stops decreasing when leaf coloration is still in process might be related to the sensitivity of NDVI to soil and litter, and leaf spectrum property change during leaf coloration. NDVI is reported to vary from 0.5 to 0.85 when LAI is 2 in response to soil lightness and land cover (Gao et al., 2000) and ground brown millet litter produce great vegetation equivalent noise for NDVI (Van Leeuwen & Huete, 1996). As for leaf spectrum properties, when leaves turn from green to yellow or red, NDVI shows obvious decreases (Motohka et al., 2010). However, the NDVI response of maples, which are dominant species in both sites, is different. Although NDVI still significantly declines in the early phase of senescence (colors turning from green to yellow), NDVI increases when color changes from yellow to red (Junker & Ensminger, 2016), which can be related with the increase of anthocyanins (Vina & Gitelson, 2011). The increase of red leaf NDVI may offset the decrease of yellow leaf NDVI, resulting in NDVI declines stopping in the second transition of leaf coloration. However, these speculations need further examination. As for EVI, it declines after full leaf coloration and sometimes even after full leaf fall, considering EVI is not sensitive to coniferous late autumn phenology since they don't change color (Huete et al., 2002; Yuan et al., 2018), this decline may be more related to the understory. EVI reduces sensitivity to soil background while keeping the sensitivity to vegetation by incorporating the blue band (Huete et al., 2002), which means it may detect understory vegetation under open canopy in late autumn with low noise. From 2010 to 2013, after full leaf coloration, this decline lasts for nine days on average in the north site and twelve days on average in south site until understory senescence and EVI loses all vegetation signals (Table 6).

In earlier comparisons, the start and middle of autumn derived from NDVI showed better consistency with the first and second transition of leaf coloration and leaf fall than EVI. Based on previous analyses, the higher consistency of early transition dates may be a result of both NDVI decrease and ground bottom-to-top observed leaf coloration starting later than the leaf coloration of top canopy. However, this phenomenon doesn't exist at the end of progression, so the differences between the bias between end of autumn, derived from NDVI and EVI respectively, and the third transition of leaf coloration or leaf fall become smaller (Table 6, Figure 5). The delayed observed leaf coloration and NDVI start-of-decrease, and the closeness of bias in the end of progression contribute to the overall similarity of NDVI and observation derived progression rate (Table 7, Table 8).

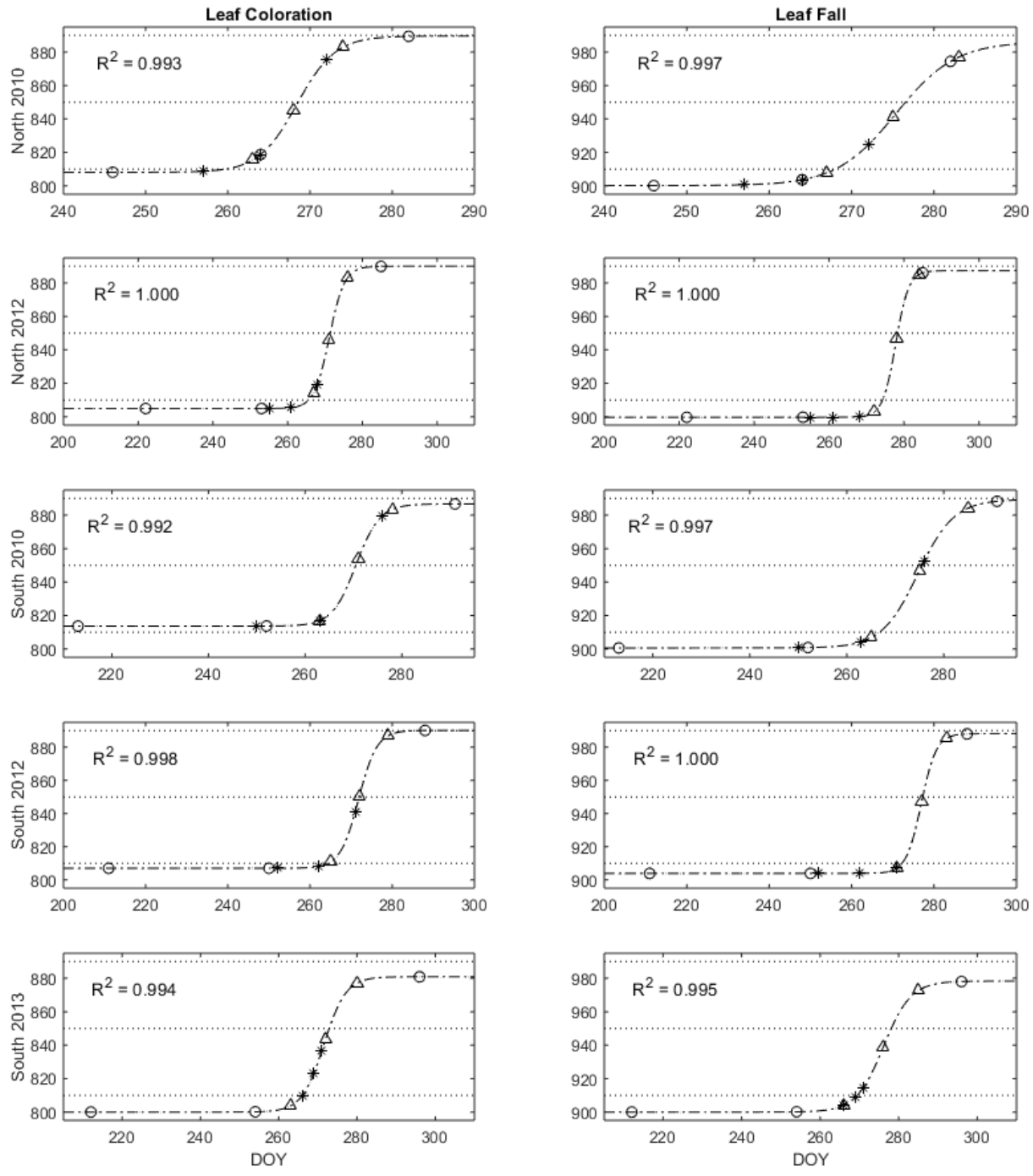

Figure 7. Field phenology correspondence with transition dates derived from four indirect approaches.

Dot-dash lines are the fitted curves of field phenology, with leaf coloration in the left column and leaf fall in the right column. R square values shown are the goodness of fit of these curves. The horizontal axes show transition dates derived from different approaches while the vertical axes show the field phenology value on that day. Circles

represent start, middle and end of autumn derived from normalized EVI, stars represent transitions derived from normalized NDVI and triangles represent field phenology. The three dotted lines in each chart represent 10%, 50% and 90% of leaf coloration or leaf fall, based on the observation scheme.

6.3 Field observation and carbon flux measurements

6.3.1 The variation of carbon flux during observed autumn progression

As expected, photosynthesis declines during leaf coloration and leaf fall. In 2012, NEE derived end of autumn (EOA) and the duration of leaf coloration and leaf fall are close, indicating leaf coloration and leaf fall happen at the end of NEE increase. Specifically, EOA derived from NEE is one day later than the first transition of leaf coloration in the north site and six days later than that for the south site. From the first to the last leaf coloration transition, NEE increases from -0.70 to -0.45 $\mu molCO_2\, m^{-2}\, s^{-1}$ in the north site while from -0.77 to -0.38 $\mu molCO_2\, m^{-2}\, s^{-1}$ in south site. During the entire leaf fall progress, conversely, NEE increases from -0.55 to -0.28 $\mu molCO_2\, m^{-2}\, s^{-1}$ in the north site while from -0.58 to -0.30 $\mu molCO_2\, m^{-2}\, s^{-1}$ in the south site. This tiny change is due to: 1) the duration of leaf coloration and leaf fall only plays a small role in the duration of NEE increase; and 2) NEE increases are slow near EOA. Meanwhile, although GPP doesn't produce seasonal markers, the GPP differences between the first and last transition of leaf coloration and leaf fall are trivial, indicating GPP decrease has almost stopped during leaf coloration and leaf fall. In particular, during the entire leaf coloration progress, GPP decreases by 0.55 $\mu molCO_2\, m^{-2}\, s^{-1}$ in the north site and by 0.84 $\mu molCO_2\, m^{-2}\, s^{-1}$ in the south site. During leaf fall progress, GPP decreases by 0.55 $\mu molCO_2\, m^{-2}\, s^{-1}$ in the north site and by 0.57 $\mu molCO_2\, m^{-2}\, s^{-1}$ in the south site.

In 2013, leaf coloration and leaf fall occur between NEE derived middle and end of autumn, and GPP derived middle of autumn overlaps with leaf coloration and leaf fall duration in

the south site. NEE increases from -1.92 to -1.00 $\mu molCO_2\ m^{-2}\ s^{-1}$ during leaf coloration and from -1.67 to -0.79 $\mu molCO_2\ m^{-2}\ s^{-1}$ during leaf fall; GPP decrease from 8.50 to 5.41 $\mu molCO_2\ m^{-2}\ s^{-1}$ during leaf coloration and form 7.78 to 4.58 $\mu molCO_2\ m^{-2}\ s^{-1}$ during leaf fall. Compared with 2012, leaf coloration and leaf fall in 2013 occur in earlier stages of the carbon exchange decline, and the NEE and GPP differences between the first and third transition of leaf coloration and leaf fall are greater (Figure 8). In these two years, photosynthesis consistently starts to decrease before the first transitions of leaf coloration and leaf fall, while carbon exchange keeps declining even after full leaf coloration and full leaf fall.

6.3.2 The reason of mismatch between field observation and carbon flux measurements

The time mismatch before the first transition of leaf coloration may partly be caused by the asynchronous canopy senescence. The canopy top senescence starts before leaf coloration can be observed from the bottom, which contributes to the carbon exchange decline before observed leaf coloration. In addition, photosynthesis is reported to decline before coloration. For example, maximum rate of carboxylation, which is an indicator of photosynthetic capacity, starts to decrease since mid-summer when leaf nitrogen and leaf area are constant (Wilson et al., 2001); photosynthetic capacity per unit area of R. Maple and S. Maple in Wisconsin peak in summer (Reich et al., 1991). Largest reductions of maximum carboxylation rate occur 6-8 weeks before observed leaf progression (Wilson et al., 2000b), corresponding with NEE derived start of autumn occurring 9-11 weeks in average before the first transition of leaf coloration in year-to-year comparison, and 6 weeks earlier in long-term comparison in this study (Table 6, Figure 5). Photosynthesis decreases after the summer solstice (when leaves are still green) can be explained by the shortening photoperiod (Bauerle et al., 2012). Except for photoperiod, photosynthetic capacity is also limited by drought and temperature (Weber & Gates, 1990; Wilson et al., 2000a;

Busch et al., 2008). In addition to environmental factors, photosynthetic capacity declines as leaves grow older, and leaf thickness also impacts photosynthesis (Reich et al., 1991; Wilson et al., 2000b; Peterson et al., 2001). These factors may explain the overall decrease of carbon exchange before observed leaf coloration.

During visual leaf progression, as expected, carbon exchange keeps decreasing with the decomposition of chlorophyll. However, NEE and GPP keep declining after full leaf coloration and full leaf fall, when NEE is still negative and GPP is still positive, indicating the photosynthesis of coniferous and understory in the ecosystem overrides the overall respiration. The phenology of understory vegetation, unfortunately, is not recorded in this study. However, previous research suggests understory shrubs last longer than canopy, contributing to ecosystem carbon deposition after full leaf fall (Gill et al., 1998; Kawamura et al., 2001). The photosynthesis of evergreen species, on the other hand, is not related to their canopy phenology, but is more influenced by temperature (Tanja et al., 2003; Richardson et al., 2009). Therefore, the decline of carbon exchange after full leaf fall can be caused by shrub autumn progression as well as declining coniferous photosynthesis under decreasing temperature.

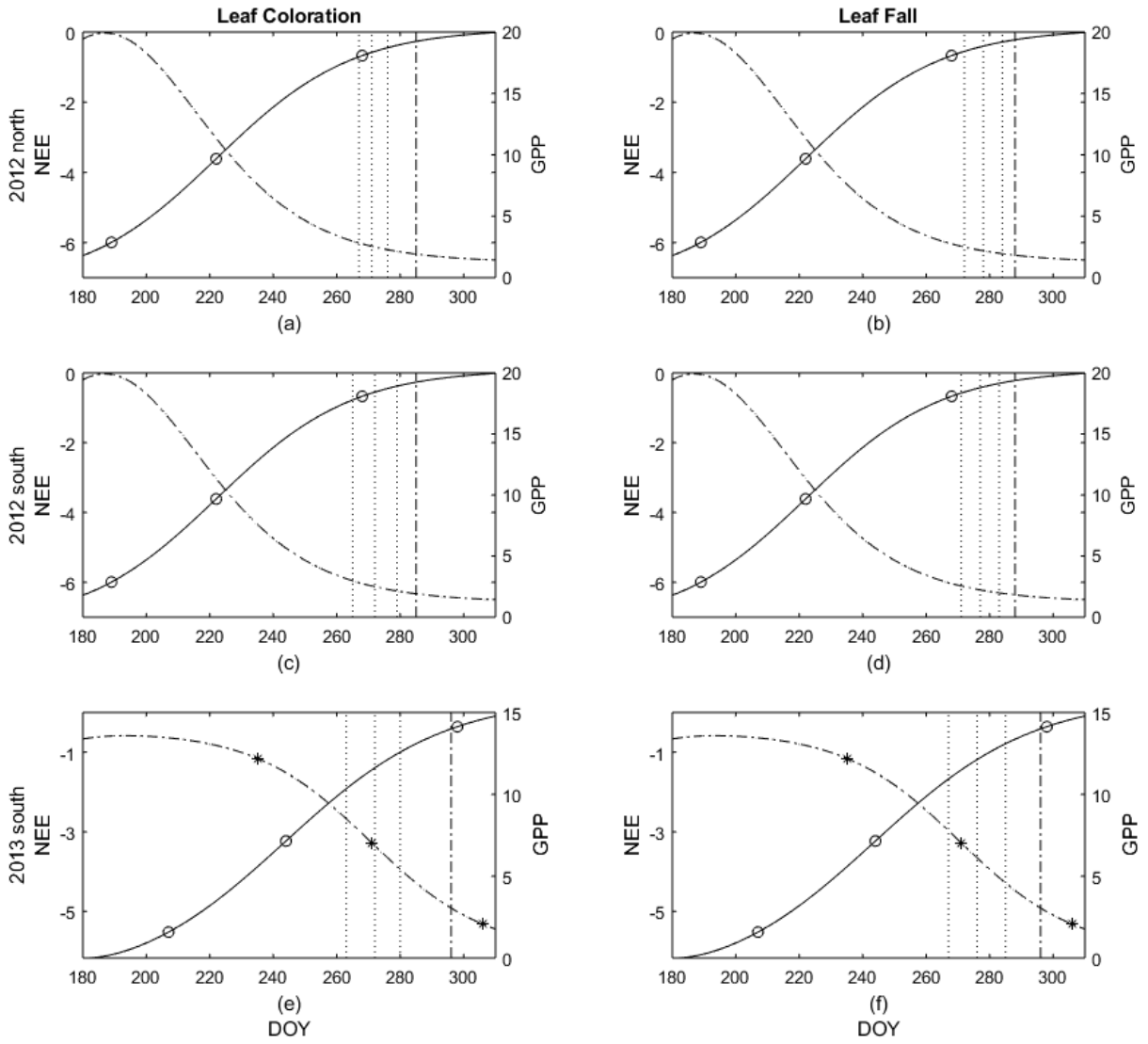

Figure 8. NEE increase and GPP decrease variation.

The solid lines show NEE while dot-dash lines show GPP. The unit of NEE and GPP are both $\mu molCO_2\ m^{-2}\ s^{-1}$. The vertical dotted lines correspond with the first, second and third transitions of leaf coloration and leaf fall progress, while vertical dash-dot lines are EOA derived from EVI. Hollow circles on NEE curves are start, middle and end of autumn derived from NEE, similarly, black asterisks on GPP curves are start, middle and end of autumn derived from GPP. 2010 is not included since there is no reliable data.

6.4 Satellite data and carbon flux measurements

For both sites, the progression parameters derived from NDVI congregate on the upper right corner of Figure 9, while the data points of other three approaches mix and concentrate in the lower parts of the graphs. This distribution indicates EVI has higher consistency with NEE and GPP than NDVI. This conclusion is supported by Wu et al. (2017), suggesting NDVI derived phenology has poor correlation with carbon derived end of growing season, especially for mixed forests; and Peng et al. (2017), suggesting EVI based spring onset has higher consistency with carbon flux measurements than NDVI.

The discrepancy between NDVI and carbon flux in early autumn progression could be caused by NDVI saturation at high LAI, as discussed earlier. Furthermore, NDVI shows a logarithmic relationship with chlorophyll content in sugar maple (Junker & Ensminger, 2016) and grassland, shrubs and trees in California (Gamon et al., 1995). NDVI also saturates when chlorophyll content is as low as 7.0 nmol/cm^2 in horse chestnut and Norway maple (Gitelson & Merzlyak, 1994) and the overall correlation between NDVI and pigment content is poor in Eucalyptus species (Datt, 1998). Compared with NDVI, EVI has a similar log relationship with chlorophyll content but has a higher saturation threshold (Schlemmer et al., 2013); and when chlorophyll content is greater than 1 g/m^2, EVI crop canopy noise is lower than NDVI (Peng et al., 2017). These features indicate EVI has higher accuracy in estimating chlorophyll content than NDVI in highly vegetated areas. This phenomenon probably contributes to its higher consistency with carbon flux variation than NDVI, especially in terms of SOA when vegetation thrives (Table 6, Figure 5 (a)(b)). However, it should be noted that the green band is not included in either EVI or NDVI, which is sensitive to chlorophyll (Gitelson & Merzlyak, 1994; Datt, 1998). Indices that include the green spectrum show higher consistency with chlorophyll content

variation than NDVI (Gitelson et al., 1996; Lichtenthaler et al., 1996; Motohka et al., 2010), and lower noise than EVI (Peng et al., 2017). Therefore, EVI and NDVI are not the best indices to extract chlorophyll content. Furthermore, chlorophyll content alone can't determine the intensity of photosynthesis. Climate factors such as photoperiod, temperature, drought and physiological factors such as leaf age and leaf thickness, as discussed earlier, can impact photosynthesis intensity. These factors may lead to the start of autumn gaps between VIs and carbon flux indices in early autumn progression (Table 6, Figure 5 (a)(b)).

By the end of autumn progression, NDVI is interfered with by canopy background and fails to detect vegetation signals, which result in further discrepancies between NDVI and carbon flux indices. EVI derived end of autumn tends to occur later than full leaf fall, when carbon exchange declines at a slow pace (Figure 8). After full leaf coloration and full leaf fall, EVI keeps following at least a portion of shrub progression, during which period coniferous photosynthesis declines decline with cooling temperature until losing the vegetation signal altogether, as discussed earlier. This result in the higher temporal consistency with carbon flux indices than NDVI. However, since there is no available data on shrub phenology, it can't be determined whether understory vegetation is still green when EVI stops decreasing.

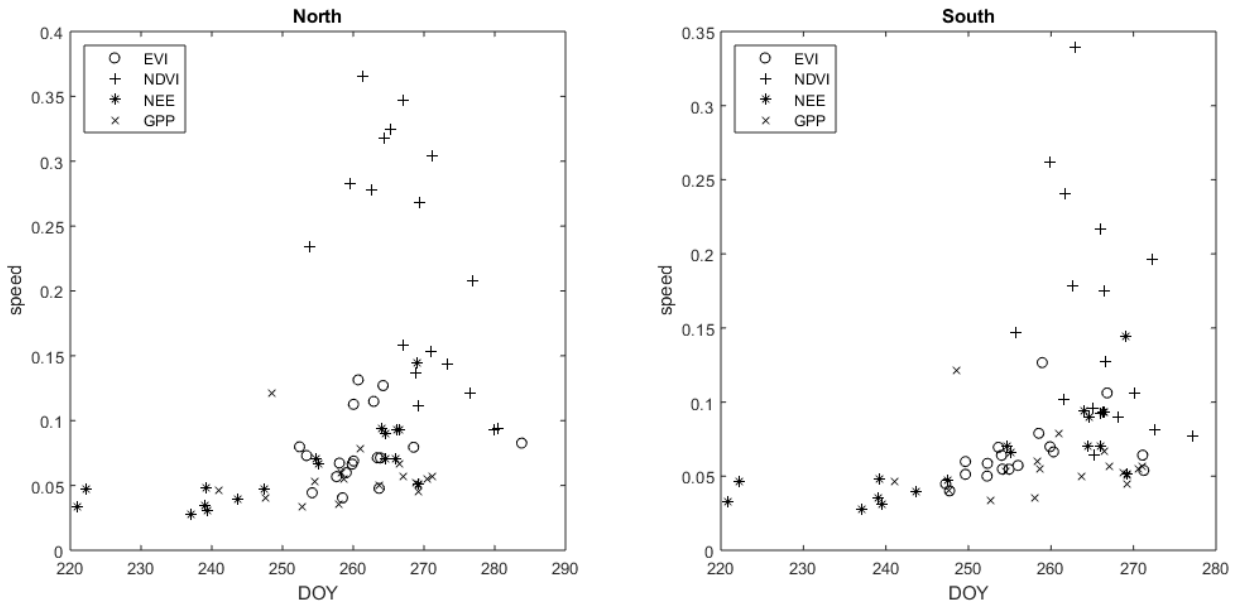

Figure 9. Middle of autumn and progression rate parameter distribution of four indirect measurements (normalized NDVI, normalized EVI, NEE and GPP).

The progression parameters derived from NDVI congregate on the upper right corner, while the data points of other three approaches mix and concentrate in the lower parts of the graphs.

7. Conclusions

7.1 Summery of findings

First, both satellite data and carbon data time series were normalized and compared with the raw time series. When normalization didn't reduce data accuracy, then normalized time series were applied to further analysis so as to simplify the fitting model. Otherwise, raw time series were applied. As a result, normalized time series of satellite data and raw time series of carbon data were chosen for analysis.

NDVI and EVI were selected for satellite data, and NEE and GPP were selected for carbon data. Together with LC and LF data, six types of time series were generated. For each time series, three transition points and progression rate were derived. For satellite data and carbon data, these transition points represented SOA, MOA and EOA respectively; while for field data, these transition points represented three phases in the LC and LF processes.

When field data were available, year-specific comparisons were conducted. NDVI showed the highest consistency with LC and LF time series, while NEE showed the lowest consistency. EVI performed better than GPP in estimating progression rate. When field data were not available, then long-term comparisons between satellite data and carbon data were conducted. The average transition dates of existing field data were used as references. Summarizing transition dates and progression rate, NDVI was closest to LC and LF processes. When field data were not considered, satellite data were compared directly to carbon data. The progression rate derived from NDVI was the fastest, and the progression rate derived from EVI, NEE and GPP didn't differ a lot.

Based on the comparative results, I have concluded that NDVI is the best approach among the selected four in estimating LC and LF. However, in the discussion section, I investigated the proportion of LC and LF (corresponding with SOA, MOA and EOA derived from these four datasets) to get more information. Both NDVI and EVI detected earlier autumn progression than field observation, which may relate to some species undergoing senescence from top to bottom. Furthermore, EVI tends to detect earlier senescence than NDVI. In the later half of senescence, NDVI loses canopy signal before senescence is complete while EVI keeps decreasing. The performance difference at the start and end of senescence suggests NDVI is less sensitive to canopy change than EVI. Therefore, both NDVI and field observation detect later senescence than EVI, which leads to the greater consistency between NDVI and field data.

In the result, carbon data showed greater differences with field data in terms of transition dates and senescence rate. These discrepancies were further analyzed in the discussion. In early autumn, NEE starts to increase and GPP starts to decrease before visual leaf senescence starts. Part of the reason is some species start coloration from the top, which is detected by CO_2 variation but not field observations, as mentioned earlier. Apart from that, photosynthesis is reported to decline before coloration due to photoperiod, temperature, water insufficiency and leaf property changes. In late autumn, the decline of coniferous and shrubs photosynthesis may also result in the changes in NEE and GPP after full leaf fall. When comparing satellite data and carbon data directly, EVI showed higher consistency with carbon data, which may relate to its higher sensitivity to LC in early autumn and lower noise interference in late autumn.

The major limitation of this project was lack of data. First, the field data period didn't overlap completely with the leaf visual senescence period. The observations could start after LC starts, or end before LF ends. As a result, the estimation of LC and LF transition points could be

imprecise. Furthermore, LC and LF proportion corresponding with the first transitions may be overestimated while the proportion corresponding with the third transition may be underestimated. Second, plant asynchronous senescence may lead to the difference between field data, satellite data and carbon data in early autumn, but there is no direct record on the senescence properties of the studied plants. Third, shrubs and coniferous trees are important factors influencing vegetation indices and carbon exchange in late autumn, especially after deciduous senescence is complete. However, there is no available record on shrubs and coniferous trees. Therefore, the explanation of differences among field data, satellite data and carbon data in late autumn is limited to theoretical speculations.

7.2 Future Research

The limitation of relative records on canopy asynchronous senescence, early and late autumn phenology and understory phenology makes it difficult to verify the speculations in this thesis. Therefore, further research, if possible, should focus on supplementation of related field records. These records include (1) deciduous species autumn phenology time series with longer duration, which start earlier and end later than the ones used in this project. These records would provide us with more precise information on the time of start and end of leaf coloration and leaf fall, as well as on the rate of canopy senescence; (2) the senescence pattern of different deciduous species (top to bottom or bottom to top). This information will help explain the differences found between bottom-to-top field observation and top-to-bottom satellite data. In addition, the senescence pattern may also partly contribute to the earlier decrease of carbon exchange than the start of field observed senescence. Therefore, if this information is available, identification of the partial contribution of senescence pattern, vegetation index sensitivity to vegetation and environmental interfere in the difference between field observation and satellite

data may be possible. Similarly, estimates of the partial contribution of senescence pattern and plant physiology (when photosynthesis decrease without visual senescence) in the difference between carbon flux measurement and field observation can also be produced; and (3) the phenology records of understory including shrubs can be recorded, which may help explain the decrease of EVI and carbon flux measurements after full leaf coloration and full leaf fall.

References

Ahas, R., & Aasa, A. (2006). The effects of climate change on the phenology of selected estonian plant, bird and fish populations. *International Journal of Biometeorology, 51*(1), 17-26. doi:10.1007/s00484-006-0041-z.

Ahl, D. E., Gower, S. T., Burrows, S. N., Shabanov, N. V., Myneni, R. B., & Knyazikhin, Y. (2006). Monitoring spring canopy phenology of a deciduous broadleaf forest using modis. *Remote Sensing of Environment, 104*(1), 88-95. doi:https://doi.org/10.1016/j.rse.2006.05.003.

Angert, A., Biraud, S., Bonfils, C., Henning, C. C., Buermann, W., Pinzon, J., et al. (2005). Drier summers cancel out the co2 uptake enhancement induced by warmer springs. *Proceedings of the National Academy of Sciences of the United States of America, 102*, 10823-10827.

Aono, Y., & Omoto, Y. (1994). Estimation of temperature at kyoto since the 11th century using flowering data of cherry trees in old documents. *Journal of Agricultural Meteorology, 49*(4), 263-272. doi:10.2480/agrmet.49.263.

Baldocchi, D., Falge, E., Gu, L., Olson, R., Hollinger, D., Running, S., et al. (2001). Fluxnet: A new tool to study the temporal and spatial variability of ecosystem-scale carbon dioxide, water vapor, and energy flux densities. *Bulletin of the American Meteorological Society, 82*(11), 2415-2434. doi:10.1175/1520-0477(2001)082<2415:fantts>2.3.co;2.

Baldocchi, D. D. (2003). Assessing the eddy covariance technique for evaluating carbon dioxide exchange rates of ecosystems: Past, present and future. *Global Change Biology, 9*, 479-492.

Bauerle, W. L., Oren, R., Way, D. A., Qian, S. S., Stoy, P. C., Thornton, P. E., et al. (2012). Photoperiodic regulation of the seasonal pattern of photosynthetic capacity and the implications for carbon cycling. *Proceedings of the National Academy of Sciences, 109*, 8612-8617.

Beaubien, E. G., & Freeland, H. J. (2000). Spring phenology trends in alberta, canada: Links to ocean temperature. *International Journal of Biometeorology, 44*(2), 53-59. doi:10.1007/s004840000050.

Beaubien, E. G., & Johnson, D. L. (1994). Flowering plant phenology and weather in alberta, canada. *International Journal of Biometeorology, 38*(1), 23-27. doi:10.1007/bf01241800.

Beck, P. S. A., Atzberger, C., Høgda, K. A., Johansen, B., & Skidmore, A. K. (2006). Improved monitoring of vegetation dynamics at very high latitudes: A new method using modis ndvi. *Remote Sensing of Environment, 100*(3), 321-334. doi:https://doi.org/10.1016/j.rse.2005.10.021.

Bradley, N. L., Leopold, A. C., Ross, J., & Huffaker, W. (1999). Phenological changes reflect climate change in wisconsin. *Proceedings of the National Academy of Sciences, 96*, 9701-9704.

Burrows, S. N., Gower, S. T., Clayton, M. K., Mackay, D. S., Ahl, D. E., Norman, J. M., et al. (2002). Application of geostatistics to characterize leaf area index (lai) from flux tower to landscape scales using a cyclic sampling design. *Ecosystems, 5*(7), 0667-0679. doi:10.1007/s10021-002-0110-z.

Busch, F., Huner, N. P., & Ensminger, I. (2008). Increased air temperature during simulated autumn conditions impairs photosynthetic electron transport between photosystem ii and photosystem i. *Plant Physiol, 147*(1), 402-414. doi:10.1104/pp.108.117598.

Caffarra, A., & Donnelly, A. (2011). The ecological significance of phenology in four different tree species: Effects of light and temperature on bud burst. *Int J Biometeorol, 55*(5), 711-721. doi:10.1007/s00484-010-0386-1.

Caffarra, A., Donnelly, A., Chuine, I., & Jones, M. B. (2011). Modelling the timing of betula pubescens budburst. I. Temperature and photoperiod: A conceptual model. *Climate Research, 46*(2), 147-157.

Cao, M., Prince, S. D., Small, J., & Goetz, S. J. (2004). Remotely sensed interannual variations and trends in terrestrial net primary productivity 1981–2000. *Ecosystems, 7*(3), 233-242. doi:10.1007/s10021-003-0189-x.

Caspersen, J. P., & Pacala, S. W. (2001). Successional diversity and forest ecosystem function. *Ecological Research, 16*(5), 895-903. doi:10.1046/j.1440-1703.2001.00455.x.

Chapman, C. A., Chapman, L. J., Struhsaker, T. T., Zanne, A. E., Clark, C. J., & Poulsen, J. R. (2005). A long-term evaluation of fruiting phenology: Importance of climate change. *Journal of Tropical Ecology, 21*(1), 31-45. doi:10.1017/S0266467404001993.

Chen, B., Coops, N. C., Fu, D., Margolis, H. A., Amiro, B. D., Barr, A. G., et al. (2011). Assessing eddy-covariance flux tower location bias across the fluxnet-canada research

network based on remote sensing and footprint modelling. *Agricultural and Forest Meteorology, 151*(1), 87-100. doi:https://doi.org/10.1016/j.agrformet.2010.09.005.

Chen, X., & Xu, L. (2012). Phenological responses of ulmus pumila (siberian elm) to climate change in the temperate zone of china. *International Journal of Biometeorology, 56*(4), 695-706. doi:10.1007/s00484-011-0471-0.

Chmielewski, F. M., Muller, A., & Kuchler, W. (2005). Possible impacts of climate change on natural vegetation in saxony (germany). *Int J Biometeorol, 50*(2), 96-104. doi:10.1007/s00484-005-0275-1.

Chmielewski, F. M., & Rötzer, T. (2001). Response of tree phenology to climate change across europe. *Agricultural and Forest Meteorology, 108*(2), 101-112. doi:https://doi.org/10.1016/S0168-1923(01)00233-7.

Cleland, E. E., Chuine, I., Menzel, A., Mooney, H. A., & Schwartz, M. D. (2007). Shifting plant phenology in response to global change. *Trends Ecol Evol, 22*(7), 357-365. doi:10.1016/j.tree.2007.04.003.

Colombo, S. J. (1998). Climatic warming and its effect on bud burst and risk of frost damage to white spruce in canada. *The Forestry Chronicle, 74*(4), 567-577. doi:10.5558/tfc74567-4.

Cong, N., Wang, T., Nan, H., Ma, Y., Wang, X., Myneni, R. B., et al. (2013). Changes in satellite-derived spring vegetation green-up date and its linkage to climate in china from 1982 to 2010: A multimethod analysis. *Global Change Biology, 19*(3), 881-891. doi:doi:10.1111/gcb.12077.

Cramer, W., Kicklighter, D. W., Bondeau, A., Iii, B. M., Churkina, G., Nemry, B., et al. (1999). Comparing global models of terrestrial net primary productivity (npp): Overview and key results. *Global Change Biology, 5*(S1), 1-15. doi:doi:10.1046/j.1365-2486.1999.00009.x.

Dahl, A., & Langvall, O. (2008). Observations on phenology in sweden - past and present. *COST action 725: the history and current states of plant phenology in Europe*, 161-165.

Datt, B. (1998). Remote sensing of chlorophyll a, chlorophyll b, chlorophyll a+b, and total carotenoid content in eucalyptus leaves. *Remote Sensing of Environment, 66*(2), 111-121. doi:https://doi.org/10.1016/S0034-4257(98)00046-7.

De Beurs, K. M., & Henebry, G. M. (2004). Land surface phenology, climatic variation, and institutional change: Analyzing agricultural land cover change in kazakhstan. *Remote Sensing of Environment, 89*(4), 497-509. doi:10.1016/j.rse.2003.11.006.

Defila, C., & Clot, B. (2001). Phytophenological trends in switzerland. *International Journal of Biometeorology, 45*(4), 203-207. doi:10.1007/s004840100101.

Demarée, G. R., & Rutishauser, T. (2009). Origins of the word “phenology”. *Eos, Transactions American Geophysical Union, 90*(34), 291-291. doi:doi:10.1029/2009EO340004.

Desai, A. R., Bolstad, P. V., Cook, B. D., Davis, K. J., & Carey, E. V. (2005). Comparing net ecosystem exchange of carbon dioxide between an old-growth and mature forest in the upper midwest, USA. *Agricultural and Forest Meteorology, 128*(1), 33-55. doi:https://doi.org/10.1016/j.agrformet.2004.09.005.

Donnelly, A., Liu, L., Zhang, X., & Wingler, A. (2018). Autumn leaf phenology: Discrepancies between in situ observations and satellite data at urban and rural sites. *International Journal of Remote Sensing*. doi:10.1080/01431161.2018.1482021.

Donnelly, A., Salamin, N., & Jones, M. B. (2006). Changes in tree phenology: An indicator of spring warming in ireland? *Biology and Environment: Proceedings of the Royal Irish Academy, 106B*(1), 49-56.

Donnelly, A., Yu, R., Caffarra, A., Hanes, J., Liang, L., Desai, A. R., et al. (2017). Interspecific and interannual variation in the duration of spring phenophases in a northern mixed forest. *Agricultural and Forest Meteorology, 243*, 55-67. doi:https://doi.org/10.1016/j.agrformet.2017.05.007.

Dragoni, D., & Rahman, A. F. (2012). Trends in fall phenology across the deciduous forests of the eastern USA. *Agricultural and Forest Meteorology, 157*, 96-105. doi:https://doi.org/10.1016/j.agrformet.2012.01.019.

Dragoni, D., Schmid, H. P., Wayson, C. A., Potter, H., Grimmond, C. S. B., & Randolph, J. C. (2011). Evidence of increased net ecosystem productivity associated with a longer vegetated season in a deciduous forest in south-central indiana, USA. *Global Change Biology, 17*(2), 886-897. doi:doi:10.1111/j.1365-2486.2010.02281.x.

Falge, E., Baldocchi, D., Tenhunen, J., Aubinet, M., Bakwin, P., Berbigier, P., et al. (2002). Seasonality of ecosystem respiration and gross primary production as derived from fluxnet measurements. *Agricultural and Forest Meteorology, 113*(1), 53-74. doi:https://doi.org/10.1016/S0168-1923(02)00102-8.

Feng, S., & Hu, Q. (2004). Changes in agro-meteorological indicators in the contiguous united states: 1951–2000. *Theoretical and Applied Climatology, 78*(4), 247-264. doi:10.1007/s00704-004-0061-8.

Fisher, J. I., Mustard, J. F., & Vadeboncoeur, M. A. (2006). Green leaf phenology at landsat resolution: Scaling from the field to the satellite. *Remote Sensing of Environment, 100*(2), 265-279. doi:https://doi.org/10.1016/j.rse.2005.10.022.

Fitter, A. H., Fitter, R. S. R., Harris, I. T. B., & Williamson, M. H. (1995). *Relationships between first flowering date and temperature in the flora of a locality in central england.* (Vol. 16).

Galan, C., Garcia-Mozo, H., Vazquez, L., Ruiz, L., De La Guardia, C. D., & Trigo, M. M. (2005). Heat requirement for the onset of the olea europaea l. Pollen season in several sites in andalusia and the effect of the expected future climate change. *Int J Biometeorol, 49*(3), 184-188. doi:10.1007/s00484-004-0223-5.

Gamon, J. A., Field, C. B., Goulden, M. L., Griffin, K. L., Hartley, A. E., Joel, G., et al. (1995). Relationships between ndvi, canopy structure, and photosynthesis in three californian vegetation types. *Ecological Applications, 5*(1), 28-41. doi:doi:10.2307/1942049.

Gao, X., Huete, A. R., Ni, W., & Miura, T. (2000). Optical–biophysical relationships of vegetation spectra without background contamination. *Remote Sensing of Environment, 74*(3), 609-620. doi:https://doi.org/10.1016/S0034-4257(00)00150-4.

Garrity, S. R., Bohrer, G., Maurer, K. D., Mueller, K. L., Vogel, C. S., & Curtis, P. S. (2011). A comparison of multiple phenology data sources for estimating seasonal transitions in deciduous forest carbon exchange. *Agricultural and Forest Meteorology, 151*(12), 1741-1752. doi:https://doi.org/10.1016/j.agrformet.2011.07.008.

Gates, D. M. (1969). Phenology program of the ibp. *The Science Teacher, 36*(4), 28-30.

Ge, Q., Wang, H., Rutishauser, T., & Dai, J. (2015). Phenological response to climate change in china: A meta-analysis. *Global Change Biology, 21*(1), 265-274. doi:doi:10.1111/gcb.12648.

Gill, D., Amthor, J., & Bormann, F. (1998). Leaf phenology, photosynthesis, and the persistence of samplings and shrubs in a mature northern hardwood forest. *Tree Physiol., 18*(5), 281-289.

Gitelson, A., & Merzlyak, M. N. (1994). Spectral reflectance changes associated with autumn senescence of aesculus hippocastanum l. And acer platanoides l. Leaves. Spectral features and relation to chlorophyll estimation. *Journal of Plant Physiology, 143*(3), 286-292. doi:https://doi.org/10.1016/S0176-1617(11)81633-0.

Gitelson, A. A., Kaufman, Y. J., & Merzlyak, M. N. (1996). Use of a green channel in remote sensing of global vegetation from eos-modis. *Remote Sensing of Environment, 58*(3), 289-298. doi:https://doi.org/10.1016/S0034-4257(96)00072-7.

Goetz, S. J., & Prince, S. D. (1996). Remote sensing of net primary production in boreal forest stands. *Agricultural and Forest Meteorology, 78*(3), 149-179. doi:https://doi.org/10.1016/0168-1923(95)02268-6.

Goetz, S. J., & Prince, S. D. (1999). Modelling terrestrial carbon exchange and storage: Evidence and implications of functional convergence in light-use efficiency. In A. H. Fitter & D. Raffaelli (Eds.), *Advances in ecological research* (Vol. 28, pp. 57-92): Academic Press.

Goetz, S. J., Prince, S. D., Small, J., & Gleason, A. C. R. (2000). Interannual variability of global terrestrial primary production: Results of a model driven with satellite observations. *Journal of Geophysical Research: Atmospheres, 105*(D15), 20077-20091. doi:doi:10.1029/2000JD900274.

Gonsamo, A., Chen, J. M., Price, D. T., Kurz, W. A., & Wu, C. (2012). Land surface phenology from optical satellite measurement and co2 eddy covariance technique. *Journal of Geophysical Research: Biogeosciences, 117*(G3). doi:doi:10.1029/2012JG002070.

Goswami, S., Gamon, J., Vargas, S., & Tweedie, C. (2015). Relationships of ndvi, biomass, and leaf area index (lai) for six key plant species in barrow, alaska. *PeerJ PrePrints, 3*. doi:10.7287/peerj.preprints.913v1.

Goulden, M. L., Munger, J. W., Fan, S.-M., Daube, B. C., & Wofsy, S. C. (1996). Exchange of carbon dioxide by a deciduous forest: Response to interannual climate variability. *Science, 271*(5255), 1576.

Gower, S. T., Mcmurtrie, R. E., & Murty, D. (1996). Aboveground net primary production decline with stand age: Potential causes. *Trends in Ecology & Evolution, 11*(9), 378-382. doi:https://doi.org/10.1016/0169-5347(96)10042-2.

Gratani, L., Fiorentino, E., & Fida, C. (1986). Phenological behaviour as a function of temperature for several species of psammophilous vegetation. *Anales Jard. Bot. Madrid, 43*(1), 125-135.

Group, B. W. (2001). *Growth stages of mono-and dicotyledonous plants*: Federal Biological Research Centre for Agriculture and Forestry.

Hanes, J. M. (2011). *Multi-scalar analysis of spring phenology in a northern mixed forest.* (Doctor of Philosophy), University of Wisconsin-Milwaukee.

Haugen, D. E., Freeman, P. C., & Theisen, M. A. (1998). *The forest resources of the chequamegon-nicolet national forest*. Published.

Huete, A., Didan, K., Miura, T., Rodriguez, E. P., Gao, X., & Ferreira, L. G. (2002). Overview of the radiometric and biophysical performance of the modis vegetation indices. *Remote Sensing of Environment, 83*(1), 195-213. doi:https://doi.org/10.1016/S0034-4257(02)00096-2.

Hunt, E. R., & Running, S. W. (1992). Simulated dry matter yields for aspen and spruce stands in the north american boreal forest. *Canadian Journal of Remote Sensing, 18*(3), 126-133. doi:10.1080/07038992.1992.10855315.

Ipcc. (2014). *Climate change 2014: Synthesis report. Contribution of working groups i, ii and iii to the fifth assessment report of the intergovernmental panel on climate change [core writing team, r.K. Pachauri and l.A. Meyer (eds.)]*. Published.

Jiang, Z., Huete, A., Didan, K., & Miura, T. (2008). *Development of a two-band enhanced vegetation index without a blue band* (Vol. 112).

Junker, L. V., & Ensminger, I. (2016). Relationship between leaf optical properties, chlorophyll fluorescence and pigment changes in senescing acer saccharum leaves. *Tree Physiology, 36*(6), 694-711. doi:10.1093/treephys/tpv148.

Karsenty, A., Blanco, C., & Dufour, T. (2003). *Forest and climate change. Instruments related to the united nations framework convention on climate change and their potential for sustainable forest management in africa*. Published.

Kaspar, F., Zimmermann, K., & Polte-Rudolf, C. (2014). An overview of the phenological observation network and the phenological database of germany's national meteorological service (deutscher wetterdienst). *Advances in Science & Research, 11*, 93-99.

Kawamura, K., Hashimoto, Y., Sakai, T., & Akiyama, T. (2001). Effects of phenological changes of canopy leaf on the spatial and seasonal variations of understory light

environment in a cool-temperate deciduous broad-leaved forest. *JOURNAL OF THE JAPANESE FORESTRY SOCIETY, 83*(3), 231-237. doi:10.11519/jjfs1953.83.3_231.

Koike, T. (1990). Autumn coloring, photosynthetic performance and leaf development of deciduous broad-leaved trees in relation to forest succession. *Tree Physiology, 7*(1-4), 21-32. doi:10.1093/treephys/7.1-2-3-4.21.

Koike, T., Kitao, M., Maruyama, Y., Mori, S., & Lei, T. T. (2001). Leaf morphology and photosynthetic adjustments among deciduous broad-leaved trees within the vertical canopy profile. *Tree Physiology, 21*(12-13), 951-958. doi:10.1093/treephys/21.12-13.951.

Krishna Prasad, V., Badarinath, K. V. S., & Eaturu, A. (2006). Spatial patterns of vegetation phenology metrics and related climatic controls of eight contrasting forest types in india – analysis from remote sensing datasets. *Theoretical and Applied Climatology, 89*(1), 95. doi:10.1007/s00704-006-0255-3.

Lasslop, G., Reichstein, M., Papale, D., Richardson, A. D., Arneth, A., Barr, A., et al. (2010). Separation of net ecosystem exchange into assimilation and respiration using a light response curve approach: Critical issues and global evaluation. *Global Change Biology, 16*, 187-208.

Liang, L. (2009). *Landscape phenology of wisconsin's temperature mixed forest.* (Doctor of Philosophy), University of Wisconsin-Milwaukee.

Liang, L., & Schwartz, M. D. (2009). Landscape phenology: An integrative approach to seasonal vegetation dynamics. *Landscape Ecology, 24*(4), 465-472. doi:10.1007/s10980-009-9328-x.

Liang, L., Schwartz, M. D., & Fei, S. (2011). Validating satellite phenology through intensive ground observation and landscape scaling in a mixed seasonal forest. *Remote Sensing of Environment, 115*(1), 143-157. doi:https://doi.org/10.1016/j.rse.2010.08.013.

Lichtenthaler, H. K., Gitelson, A., & Lang, M. (1996). Non-destructive determination of chlorophyll content of leaves of a green and an aurea mutant of tobacco by reflectance measurements. *Journal of Plant Physiology, 148*(3), 483-493. doi:https://doi.org/10.1016/S0176-1617(96)80283-5.

Lieth, H. (1974). *Phenology and seasonality modeling* (Vol. 8).

Linkosalo, T. (1999). Regularities and patterns in the spring phenology of some boreal trees. *Silva Fennica, 33*(4), 237-245. doi:10.14214/sf.647.

Liu, L., Liang, L., Schwartz, M. D., Donnelly, A., Wang, Z., Schaaf, C. B., et al. (2015). Evaluating the potential of modis satellite data to track temporal dynamics of autumn phenology in a temperate mixed forest. *Remote Sensing of Environment, 160*, 156-165. doi:https://doi.org/10.1016/j.rse.2015.01.011.

Liu, L., Zhang, X., Yu, Y., & Donnelly, A. (2017). Detecting spatiotemporal changes of peak foliage coloration in deciduous and mixedforests across the central and eastern united states. *Environmental Research Letters, 12*. doi:10.1088/1748-9326/aa5b3a.

Liu, Q., Fu, Y., Zhu, Z., Liu, Y., Liu, Z., H, M., et al. (2016). Delayed autumn phenology in the northern hemisphere is related to change in both climate and spring phenology. *Global Change Biology, 22*, 3702-3711. doi:10.1111/gcb.13311.

Margary, I. D. (1925). *The marsham phenological record in norfolk, 1736-1925, and some others* (Vol. 52).

Menzel, A. (2003). Plant phenological anomalies in germany and their relation to air temperature and nao. *Climatic Change, 57*(3), 243-263. doi:10.1023/a:1022880418362.

Menzel, A., & Fabian, P. (1999). Growing season extended in europe. *Nature, 397*, 659. doi:10.1038/17709.

Menzel, A., Jakobi, G., Ahas, R., Scheifinger, H., & Estrella, N. (2003). Variations of the climatological growing season (1951-2000) in germany compared to other countries. *International Journal of Climatology, 23*, 793-812. doi:10.1002/joc.915.

Menzel, A., Sparks, T. H., Estrella, N., Koch, E., Aasa, A., Ahas, R., et al. (2006). European phenological response to climate change matches the warming pattern. *Global Change Biology, 12*(10), 1969-1976. doi:10.1111/j.1365-2486.2006.01193.x.

Mikami, T. (2008). Climatic variations in japan reconstructed from historical documents. *Weather, 63*(7), 190-193.

Moran, M. S., Maas, S. J., & Pinter, P. J. (1995). Combining remote sensing and modeling for estimating surface evaporation and biomass production. *Remote Sensing Reviews, 12*(3-4), 335-353. doi:10.1080/02757259509532290.

Motohka, T., Nasahara, K. N., Oguma, H., & Tsuchida, S. (2010). Applicability of green-red vegetation index for remote sensing of vegetation phenology. *Remote Sensing, 2*(10), 2369.

Moulin, S., Kergoat, L., Viovy, N., & Dedieu, G. (1997). Global-scale assessment of vegetation phenology using noaa/avhrr satellite measurements. *Journal of Climate, 10*, 1154-1170.

Myneni, R. B., Dong, J., Tucker, C. J., Kaufmann, R. K., Kauppi, P. E., Liski, J., et al. (2001). A large carbon sink in the woody biomass of northern forests. *Proceedings of the National Academy of Sciences, 98*, 14784-14789.

Myneni, R. B., Keeling, C. D., Tucker, C. J., Asrar, G., & Nemani, R. R. (1997). Increased plant growth in the northern high latitudes from 1981 to 1991. *Nature, 386*, 698. doi:10.1038/386698a0.

Nagai, S., Nasahara, K. N., Muraoka, H., Akiyama, T., & Tsuchida, S. (2010). Field experiments to test the use of the normalized-difference vegetation index for phenology detection. *Agricultural and Forest Meteorology, 150*(2), 152-160. doi:https://doi.org/10.1016/j.agrformet.2009.09.010.

Pagenkopf, T. (2010). New phenological garden supporting both the international phenological garden and the global phenological monitoring programme. *Phenology Journal, 35*.

Peng, D., Wu, C., Li, C., Zhang, X., Liu, Z., Ye, H., et al. (2017). Spring green-up phenology products derived from modis ndvi and evi: Intercomparison, interpretation and validation using national phenology network and ameriflux observations. *Ecological Indicators, 77*, 323-336. doi:https://doi.org/10.1016/j.ecolind.2017.02.024.

Peterson, A. G., Ball, J. T., Luo, Y., Field, C. B., Reich, P. B., Curtis, P. S., et al. (2001). The photosynthesis – leaf nitrogen relationship at ambient and elevated atmospheric carbon dioxide: A meta‐analysis. *Global Change Biology, 5*, 331-346.

Piao, S., Ciais, P., Friedlingstein, P., Peylin, P., Reichstein, M., Luyssaert, S., et al. (2008). Net carbon dioxide losses of northern ecosystems in response to autumn warming. *Nature, 451*(7174), 49-52. doi:10.1038/nature06444.

Reed, B., Brown, J., Vanderzee, D., Loveland, T. R., Merchant, J. W., & Ohlen, D. O. (1994). Measuring phenological variability from satellite imagery. *Journal of Vegetation Science, 5*, 703-714.

Reed, B. C. (2006). Trend analysis of time-series phenology of north america derived from satellite data. *GIScience & Remote Sensing, 43*(1), 24-38. doi:10.2747/1548-1603.43.1.24.

Reich, P., Walters, M., & Ellsworth, D. (1991). Leaf age and season influence the relationships between leaf nitrogen, leaf mass per area and photosynthesis in maple and oak trees. *14*, 251-259. doi:10.1111/j.1365-3040.1991.tb01499.x.

Richardson, A. D., Bailey, A. S., Denny, E. G., Martin, C. W., & O'keefe, J. (2006). Phenology of a northern hardwood forest canopy. *Global Change Biology, 12*(7), 1174-1188. doi:doi:10.1111/j.1365-2486.2006.01164.x.

Richardson, A. D., Black, T. A., Ciais, P., Delbart, N., Friedl, M. A., Gobron, N., et al. (2010). Influence of spring and autumn phenological transitions on forest ecosystem productivity. *Philosophical Transactions of the Royal Society B: Biological Sciences, 365*(1555), 3227-3246. doi:doi:10.1098/rstb.2010.0102.

Richardson, A. D., Hollinger, D. Y., Dail, D. B., Lee, J. T., Munger, J. W., & O'keefe, J. (2009). Influence of spring phenology on seasonal and annual carbon balance in two contrasting new england forests. *Tree Physiology, 29*(3), 321-331. doi:10.1093/treephys/tpn040.

Richardson, A. D., Hufkens, K., Milliman, T., Aubrecht, D. M., Chen, M., Gray, J. M., et al. (2018). Tracking vegetation phenology across diverse north american biomes using phenocam imagery. *Scientific Data, 5*, 180028. doi:10.1038/sdata.2018.28.

Richardson, A. D., Jenkins, J. P., Braswell, B. H., Hollinger, D. Y., Ollinger, S. V., & Smith, M.-L. (2007). Use of digital webcam images to track spring green-up in a deciduous broadleaf forest. *Oecologia, 152*(2), 323-334. doi:10.1007/s00442-006-0657-z.

Rouse, J. W., Jr., Haas, R. H., Schell, J. A., & Deering, D. W. (1974). *Monitoring vegetation systems in the great plains with erts*. Paper presented at the NASA. Goddard Space Flight Center 3d ERTS-1 Symp.

Running, S. W., Baldocchi, D. D., Turner, D. P., Gower, S. T., Bakwin, P. S., & Hibbard, K. A. (1999). A global terrestrial monitoring network integrating tower fluxes, flask sampling, ecosystem modeling and eos satellite data. *Remote Sensing of Environment, 70*(1), 108-127. doi:https://doi.org/10.1016/S0034-4257(99)00061-9.

Schaber, J., & Badeck, F.-W. (2003). Physiology-based phenology models for forest tree species in germany. *International Journal of Biometeorology, 47*(4), 193-201. doi:10.1007/s00484-003-0171-5.

Schimel, D., Pavlick, R., Fisher, J. B., Asner, G. P., Saatchi, S., Townsend, P., et al. (2015). Observing terrestrial ecosystems and the carbon cycle from space. *Global Change Biology, 21*(5), 1762-1776. doi:doi:10.1111/gcb.12822.

Schlemmer, M., Gitelson, A., Schepers, J., Ferguson, R., Peng, Y., Shanahan, J., et al. (2013). Remote estimation of nitrogen and chlorophyll contents in maize at leaf and canopy levels. *International Journal of Applied Earth Observation and Geoinformation, 25*, 47-54. doi:https://doi.org/10.1016/j.jag.2013.04.003.

Schnelle, F. (1956). Pflanzen-phänologie. Probleme der bioklimatologie bd. 3. Akadem. Verlagsges. Leipzig 1955. 299 s., 46 abb., 14 kart. *Zeitschrift für Pflanzenernährung, Düngung, Bodenkunde, 73*(2), 156-156. doi:doi:10.1002/jpln.19560730209.

Schwartz, M. (2003). *Phenology: An integrative environmental science* (Vol. 132).

Schwartz, M. D. (1990). Meteorological causes of the 1881 fire in michigan's thumb area. *Weather and Forecasting, 5*(1), 148-157. doi:10.1175/1520-0434(1990)005<0148:mcotfi>2.0.co;2.

Schwartz, M. D. (1994). Monitoring global change with phenology: The case of the spring green wave. *International Journal of Biometeorology, 38*(1), 18-22. doi:10.1007/bf01241799.

Schwartz, M. D. (1998). Green-wave phenology. *Nature, 394*, 839. doi:10.1038/29670.

Schwartz, M. D., Ahas, R., & Aasa, A. (2006). Onset of spring starting earlier across the northern hemisphere. *Global Change Biology, 12*, 343-351.

Schwartz, M. D., & Chen, X. (2002). Examining the onset of spring in china. *Climate Research, 21*(2), 157-164.

Schwartz, M. D., & Karl, T. R. (1990). Spring phenology: Nature's experiment to detect the effect of “green-up” on surface maximum temperatures. *Monthly Weather Review, 118*(4), 883-890. doi:10.1175/1520-0493(1990)118<0883:spnetd>2.0.co;2.

Sellers, P. J., Hall, F. G., Asrar, G., Strebel, D. E., & Murphy, R. E. (1992). An overview of the first international satellite land surface climatology project (islscp) field experiment (fife). *Journal of Geophysical Research: Atmospheres, 97*(D17), 18345-18371. doi:doi:10.1029/92JD02111.

Shi, A., & Marschner, P. (2017). Soil respiration and microbial biomass in multiple drying and rewetting cycles – effect of glucose addition. *Geoderma, 305*, 219-227. doi:https://doi.org/10.1016/j.geoderma.2017.06.010.

Solaymani, S. (2017). Carbon and energy taxes in a small and open country. *Global Journal of Environmental Science and Management, 3*(1), 51-62. doi:10.22034/gjesm.2017.03.01.006.

Soudani, K., Le Maire, G., Dufrêne, E., François, C., Delpierre, N., Ulrich, E., et al. (2008). Evaluation of the onset of green-up in temperate deciduous broadleaf forests derived from moderate resolution imaging spectroradiometer (modis) data. *Remote Sensing of Environment, 112*(5), 2643-2655. doi:https://doi.org/10.1016/j.rse.2007.12.004.

Sparks, T., & Collinson, N. (2008). The histroy and current status of phenological recording in the u.K. *COST action 725: the history and current states of plant phenology in Europe*, 170-173.

Sparks, T. H., Huber, K., & Croxton, P. J. (2006). Plant development scores from fixed-date photographs: The influence of weather variables and recorder experience. *International Journal of Biometeorology, 50*(5), 275-279. doi:10.1007/s00484-005-0022-7.

Tanja, S., Berninger, F., Vesala, T., Markkanen, T., Hari, P., Mäkelä, A., et al. (2003). Air temperature triggers the recovery of evergreen boreal forest photosynthesis in spring. *Global Change Biology, 9*(10), 1410-1426. doi:doi:10.1046/j.1365-2486.2003.00597.x.

Tucker, C. J., & Sellers, P. J. (1986). Satellite remote sensing of primary production. *International Journal of Remote Sensing, 7*(11), 1395-1416. doi:10.1080/01431168608948944.

USA-Npn National Coordinating Office. (2016). *USA national phenology network data product development framework and data product catalog, v 1.1. USA-npn technical series 2016-001*. Published.

Van Leeuwen, W. J. D., & Huete, A. R. (1996). Effects of standing litter on the biophysical interpretation of plant canopies with spectral indices. *Remote Sensing of Environment, 55*(2), 123-138. doi:https://doi.org/10.1016/0034-4257(95)00198-0.

Vina, A., & Gitelson, A. A. (2011). Sensitivity to foliar anthocyanin content of vegetation indices using green reflectance. *IEEE Geoscience and Remote Sensing Letters, 8*(3), 464-468. doi:10.1109/LGRS.2010.2086430.

Walkovszky, A. (1998). Changes in phenology of the locust tree (robinia pseudoacacia l.) in hungary. *International Journal of Biometeorology, 41*(4), 155-160. doi:10.1007/s004840050069.

Weber, J. A., & Gates, D. M. (1990). Gas exchange in quercus rubra (northern red oak) during a drought: Analysis of relations among photosynthesis, transpiration, and leaf conductance. *Tree Physiol., 7*, 215-225.

Wehr, R., Munger, J. W., Mcmanus, J. B., Nelson, D. D., Zahniser, M. S., Davidson, E. A., et al. (2016). Seasonality of temperate forest photosynthesis and daytime respiration. *Nature, 534*, 680. doi:10.1038/nature17966.

White, K., Pontius, J., & Schaberg, P. (2014). Remote sensing of spring phenology in northeastern forests: A comparison of methods, field metrics and sources of uncertainty. *Remote Sensing of Environment, 148*, 97-107. doi:https://doi.org/10.1016/j.rse.2014.03.017.

White, M. A., Nemani, R. R., Thornton, P. E., & Running, S. W. (2002). Satellite evidence of phenological differences between urbanized and rural areas of the eastern united states deciduous broadleaf forest. *Ecosystems, 5*(3), 260-273. doi:10.1007/s10021-001-0070-8.

White, M. A., Running, S. W., & Thornton, P. E. (1999). The impact of growing-season length variability on carbon assimilation and evapotranspiration over 88 years in the eastern us deciduous forest. *International Journal of Biometeorology, 42*(3), 139-145. doi:10.1007/s004840050097.

White, M. A., Thornton, P. E., & Running, S. W. (1997). A continental phenology model for monitoring vegetation responses to interannual climatic variability. *Global Biogeochemical Cycles, 11*(2), 217-234. doi:doi:10.1029/97GB00330.

Wilson, K. B., Baldocchi, D. D., & Hanson, P. J. (2000a). Quantifying stomatal and non-stomatal limitations to carbon assimilation resulting from leaf aging and drought in mature deciduous tree species. *Tree Physiol, 20*, 787-797.

Wilson, K. B., Baldocchi, D. D., & Hanson, P. J. (2000b). Spatial and seasonal variability of photosynthetic parameters and their relationship to leaf nitrogen in a deciduous forest. *Tree Physiology, 20*(9), 565-578. doi:10.1093/treephys/20.9.565.

Wilson, K. B., Baldocchi, D. D., & Hanson, P. J. (2001). Leaf age affects the seasonal pattern of photosynthetic capacityand net ecosystem exchange of carbon in a deciduous forest. *Plant, Cell & Environment, 24*(6), 571-583. doi:doi:10.1046/j.0016-8025.2001.00706.x.

Wolf, S., Keenan, T. F., Fisher, J. B., Baldocchi, D. D., Desai, A. R., Richardson, A. D., et al. (2016). Warm spring reduced carbon cycle impact of the 2012 us summer drought. *Proc Natl Acad Sci U S A, 113*(21), 5880-5885. doi:10.1073/pnas.1519620113.

Wu, C., Chen, J. M., Black, T. A., Price, D. T., Kurz, W. A., Desai, A. R., et al. (2013). Interannual variability of net ecosystem productivity in forests is explained by carbon flux phenology in autumn. *Global Ecology and Biogeography*, *22*(8), 994-1006. doi:doi:10.1111/geb.12044.

Wu, C., Gough, C. M., Chen, J. M., & Gonsamo, A. (2013). Evidence of autumn phenology control on annual net ecosystem productivity in two temperate deciduous forests. *Ecological Engineering*, *60*, 88-95. doi:https://doi.org/10.1016/j.ecoleng.2013.07.019.

Wu, C., Peng, D., Soudani, K., Siebicke, L., Gough, C. M., Arain, M. A., et al. (2017). Land surface phenology derived from normalized difference vegetation index (ndvi) at global fluxnet sites. *Agricultural and Forest Meteorology*, *233*, 171-182. doi:https://doi.org/10.1016/j.agrformet.2016.11.193.

Xiao, X., Hagen, S., Zhang, Q., Keller, M., & Moore, B. (2006). Detecting leaf phenology of seasonally moist tropical forests in south america with multi-temporal modis images. *Remote Sensing of Environment*, *103*(4), 465-473. doi:https://doi.org/10.1016/j.rse.2006.04.013.

Yu, R., Schwartz, M. D., Donnelly, A., & Liang, L. (2016). An observation-based progression modeling approach to spring and autumn deciduous tree phenology. *International Journal of Biometeorology*, *60*(3), 335-349. doi:10.1007/s00484-015-1031-9.

Yuan, H., Wu, C., Lu, L., & Wang, X. (2018). A new algorithm predicting the end of growth at five evergreen conifer forests based on nighttime temperature and the enhanced vegetation index. *ISPRS Journal of Photogrammetry and Remote Sensing*, *144*, 390-399. doi:https://doi.org/10.1016/j.isprsjprs.2018.08.013.

Zhang, X. (2015). Reconstruction of a complete global time series of daily vegetation index trajectory from long-term avhrr data. *Remote Sensing of Environment*, *156*, 457-472. doi:https://doi.org/10.1016/j.rse.2014.10.012.

Zhang, X., Friedl, M. A., Schaaf, C. B., & Strahler, A. H. (2004). Climate controls on vegetation phenological patterns in northern mid- and high latitudes inferred from modis data. *Global Change Biology*, *10*(7), 1133-1145. doi:doi:10.1111/j.1529-8817.2003.00784.x.

Zhang, X., Friedl, M. A., Schaaf, C. B., Strahler, A. H., Hodges, J. C. F., Gao, F., et al. (2003). Monitoring vegetation phenology using modis. *Remote Sensing of Environment*, *84*(3), 471-475. doi:https://doi.org/10.1016/S0034-4257(02)00135-9.

Zhang, X., Hodges, J. C. F., Schaaf, C. B., Friedl, M. A., Strahler, A. H., & Gao, F. (2001). *Global vegetation phenology from avhrr and modis data*. Paper presented at the Scanning the present and resolving the future. Proceedings, Sydney.

Zhang, X., Jayavelu, S., Liu, L., Friedl, M. A., Henebry, G. M., Liu, Y., et al. (2018). Evaluation of land surface phenology from viirs data using time series of phenocam imagery. *Agricultural and Forest Meteorology, 256-257*, 137-149. doi:https://doi.org/10.1016/j.agrformet.2018.03.003.

Zhao, T., & Schwartz, M. D. (2003). Examining the onset of spring in wisconsin. *Climate Research, 24*, 59-70.

Zhou, L., Tucker, C. J., Kaufmann, R. K., Slayback, D., Shabanov, N. V., & Myneni, R. B. (2001). Variations in northern vegetation activity inferred from satellite data of vegetation index during 1981 to 1999. *Journal of Geophysical Research: Atmospheres, 106*(D17), 20069-20083. doi:doi:10.1029/2000JD000115.

Appendices

Appendix A: Z values of start of autumn derived from indirect appraoches in both sites.

Year	North EVI_{nor}	South EVI_{nor}	North $NDVI_{nor}$	South $NDVI_{nor}$	NEE	GPP
1997	N/A	N/A	N/A	N/A	0.696	-0.123
1998	N/A	N/A	N/A	N/A	0.885	0.012
1999	N/A	N/A	N/A	N/A	1.026	0.617
2000	0.246	-1.774	0.412	0.900	0.932	-0.257
2001	-0.100	0.491	1.552	1.479	1.545	0.617
2002	1.006	1.623	0.032	0.553	0.602	0.483
2003	-1.758	1.925	-1.299	0.090	-1.190	-0.594
2004	-1.827	-1.019	0.412	-0.489	-0.530	0.214
2005	-0.860	0.717	0.032	-0.026	N/A	N/A
2006	0.798	0.793	-0.348	0.321	-0.860	-2.141
2007	1.006	0.113	-2.249	-0.952	-0.719	-1.132
2008	-0.791	-0.491	-0.729	-0.836	0.130	-0.257
2009	1.904	1.170	-0.158	-0.604	0.366	2.635
2010	1.213	-0.491	0.222	0.206	N/A	N/A
2011	-0.238	-1.095	0.792	0.784	-1.709	-1.064
2012	-0.445	-0.642	-0.158	0.437	-1.567	N/A
2013	-0.307	-0.566	0.982	2.058	-0.719	0.415
2014	-0.307	-0.944	-0.919	-2.109	0.083	-0.190
2015	0.798	0.566	1.933	0.090	N/A	0.483
2016	0.177	-0.113	0.222	-1.067	1.026	0.281
2017	-0.514	-0.264	-0.729	-0.836	N/A	N/A

EVI_{nor} = normalized EVI, $NDVI_{nor}$ = normalized NDVI; N/A = not applicable.

Appendix B: Z values of middle of autumn derived from indirect appraoches in both sites.

Year	North EVI_{nor}	South EVI_{nor}	North $NDVI_{nor}$	South $NDVI_{nor}$	NEE	GPP
1997	N/A	N/A	N/A	N/A	0.855	0.890
1998	N/A	N/A	N/A	N/A	0.793	0.890
1999	N/A	N/A	N/A	N/A	0.855	0.018
2000	0.370	-1.471	-0.527	-0.634	0.732	-0.200
2001	-0.197	0.390	0.323	1.167	1.040	0.563
2002	0.228	0.247	0.323	0.167	0.732	-1.398
2003	-1.046	1.392	0.039	0.167	-0.808	-0.744
2004	-0.338	0.819	1.172	1.367	-1.054	0.890
2005	0.370	1.964	1.597	2.168	N/A	N/A
2006	-0.197	-0.183	-0.810	-1.234	-0.808	-1.398
2007	-0.055	-0.469	-2.085	-2.035	-0.315	-0.309
2008	-0.480	-0.326	0.039	-0.033	0.178	0.345
2009	**3.201**	1.964	1.597	0.367	1.040	0.999
2010	0.370	-0.756	-0.669	-0.634	N/A	N/A
2011	-0.197	-1.042	-0.244	-0.033	-1.917	-0.962
2012	-1.188	-1.042	-1.094	-0.834	-1.855	-2.161
2013	-0.480	-0.469	0.039	0.567	-0.500	1.108
2014	-1.329	-0.756	-1.235	-0.233	0.178	-0.309
2015	1.077	0.390	1.172	0.767	N/A	1.108
2016	0.228	-0.469	0.606	-0.834	0.855	0.672
2017	-0.338	-0.183	-0.244	-0.233	N/A	N/A

EVI_{nor} = normalized EVI, $NDVI_{nor}$ = normalized NDVI; N/A = not applicable. Values greater than three were bolded.

Appendix C: Z values of end of autumn derived from indirect appraoches in both sites.

Year	North EVI_{nor}	South EVI_{nor}	North $NDVI_{nor}$	South $NDVI_{nor}$	NEE	GPP
1997	N/A	N/A	N/A	N/A	0.225	0.986
1998	N/A	N/A	N/A	N/A	-0.378	0.722
1999	N/A	N/A	N/A	N/A	-0.378	-0.927
2000	0.150	0.250	-0.801	-1.182	-0.550	-0.268
2001	-0.111	-0.043	-0.231	-0.005	-0.808	-0.202
2002	-0.981	-1.801	0.340	-0.341	0.139	-2.445
2003	1.020	-0.727	0.665	0.079	-0.722	-0.466
2004	1.803	2.496	1.154	1.425	0.741	0.590
2005	1.542	1.812	1.888	1.930	N/A	N/A
2006	-1.242	-0.727	-0.883	-1.266	1.515	-0.004
2007	-1.416	-0.825	-1.453	-1.098	0.139	1.315
2008	0.324	0.152	0.340	0.584	-0.464	0.392
2009	1.542	1.129	1.888	0.836	1.601	-1.719
2010	-1.068	-0.434	-0.801	-0.678	N/A	N/A
2011	-0.024	-0.141	-0.638	-0.593	-0.464	1.118
2012	-0.807	-0.727	-1.127	-1.098	-2.098	N/A
2013	-0.198	0.054	-0.312	-1.098	0.483	0.524
2014	-1.155	0.250	-1.127	1.425	-0.636	-0.466
2015	0.237	-0.239	0.502	0.668	2.032	0.590
2016	0.150	-0.532	0.584	-0.005	-0.378	0.260
2017	0.237	0.054	0.014	0.416	N/A	N/A

EVI_{nor} = normalized EVI, $NDVI_{nor}$ = normalized NDVI; N/A = not applicable. Values greater than three were bolded.

Appendix D: Z values of progressioin rates derived from indirect appraoches in both sites.

Year	North EVI_{nor}	South EVI_{nor}	North $NDVI_{nor}$	South $NDVI_{nor}$	NEE	GPP
1997	N/A	N/A	N/A	N/A	0.205	0.385
1998	N/A	N/A	N/A	N/A	0.853	0.306
1999	N/A	N/A	N/A	N/A	0.965	-0.083
2000	-0.231	-0.953	1.128	0.850	0.978	0.243
2001	-0.320	0.063	0.907	0.037	2.653	0.076
2002	1.375	2.905	-0.704	-0.085	0.202	-0.680
2003	-1.223	1.940	-1.148	-0.358	-0.528	0.271
2004	-1.366	-1.178	-1.045	-0.619	-0.952	0.281
2005	-1.096	-0.527	-1.332	-0.639	N/A	N/A
2006	1.292	0.655	0.631	0.406	-1.091	0.448
2007	1.987	0.209	0.166	-0.247	-0.561	0.523
2008	-0.762	-0.489	-0.872	-0.553	0.080	0.315
2009	0.189	-0.042	-1.344	-0.567	-0.413	**-3.857**
2010	1.825	-0.304	1.049	-0.068	N/A	N/A
2011	-0.408	-0.652	1.364	0.152	-1.012	0.549
2012	-0.165	-0.245	1.563	0.288	-0.564	0.364
2013	-0.378	-0.486	0.522	**3.622**	-0.798	0.247
2014	0.085	-0.708	0.685	-0.712	0.215	0.176
2015	0.073	0.227	-0.115	-0.474	-1.199	0.221
2016	-0.226	-0.047	-0.804	-0.499	0.965	0.217
2017	-0.651	-0.369	-0.652	-0.535	N/A	N/A

EVI_{nor} = normalized EVI, $NDVI_{nor}$ = normalized NDVI; N/A = not applicable. Values greater than three were bolded.